Accepted Manuscript

Design, synthesis and biological evaluation of imine resveratrol derivatives as multi-targeted agents against Alzheimer's disease

Su-Yi Li, Xiao-Bing Wang, Ling-Yi Kong

PII: S0223-5234(13)00719-8

DOI: 10.1016/j.ejmech.2013.10.068

Reference: EJMECH 6531

To appear in: *European Journal of Medicinal Chemistry*

Received Date: 16 August 2013

Revised Date: 26 September 2013

Accepted Date: 28 October 2013

Please cite this article as: S.-Y. Li, X.-B. Wang, L.-Y. Kong, Design, synthesis and biological evaluation of imine resveratrol derivatives as multi-targeted agents against Alzheimer's disease, *European Journal of Medicinal Chemistry* (2013), doi: 10.1016/j.ejmech.2013.10.068.

Graphical abstract

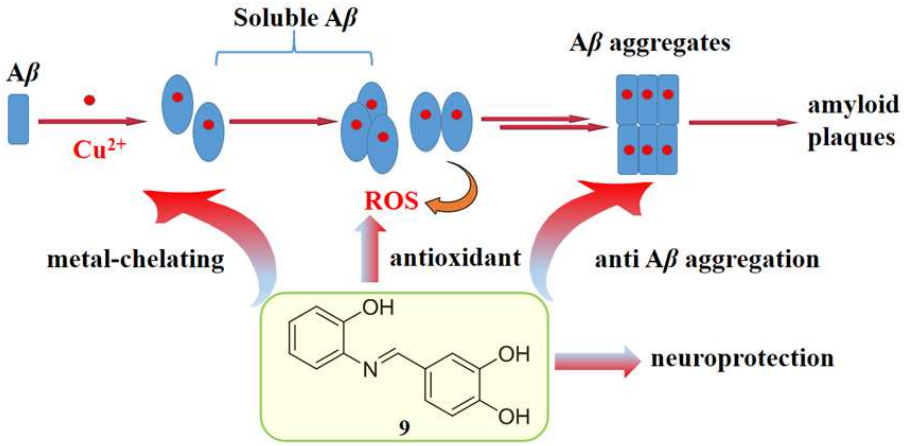

A series of imine resveratrol derivatives were designed, synthesized, and evaluated as multi-targeted compounds for the treatment of AD. **9** might be a promising compound for further study.

Design, synthesis and biological evaluation of imine resveratrol derivatives as multi-targeted agents against Alzheimer's disease

Su-Yi Li, Xiao-Bing Wang, Ling-Yi Kong *

State Key Laboratory of Natural Medicines, Department of Natural Medicinal Chemistry, China Pharmaceutical University, 24 Tong Jia Xiang, Nanjing 210009, People's Republic of China

* *Corresponding Author. Tel/Fax: +86-25-83271405; E-mail: cpu_lykong@126.com (Ling-Yi Kong);*

Abstract

A series of imine resveratrol derivatives (**1**-**20**) have been designed, synthesized, and evaluated as multi-targeted compounds for the treatment of Alzheimer's disease (AD). In vitro studies show that most of the molecules exhibit a significant ability to inhibit self-induced and Cu^{2+}-induced *β*-amyloid ($A\beta_{1-42}$) aggregation, and to function as potential antioxidants and biometal chelators. In particular, compound **9** is a potential lead compound for AD treatment (for compound **9**, IC_{50} = 14.1 μM for the antioxidant activity using DPPH free radical method; 64.6% at 20 μM for self-induced A*β* aggregation). Moreover, it is capable of decreasing reactive oxygen species (ROS) induced by Cu-A*β* and shows good neuroprotective effects in human SH-SY5Y neuroblastoma cells. Taken together, these results suggest that **9** might be a promising lead compound for AD treatment.

Key words: Alzheimer's disease, resveratrol derivatives, antioxidant, *β*-amyloid aggregation, metal chelator, neuroprotection.

1. Introduction

Alzheimer's disease (AD), is an age-related neurodegenerative disease characterized by the progressive loss of memory, decline in language skills, and other cognitive impairments [1, 2]. Although the etiology of AD still remains elusive, several factors such as amyloid-β (Aβ) deposits, τ-protein aggregation, oxidative stress, and low levels of acetylcholine (ACh) are considered to play significant roles in the pathophysiology of AD [3, 4]. Among the multiple factors that induce AD, the Aβ hypothesis is considered the most important and pivotal in particular. The "Aβ hypothesis" states that the development of AD is driven by the accumulation and deposition of Aβ peptide aggregates in the brain [5]. Aβ peptides are produced as a result of the abnormal cleavage of the amyloid precursor peptide (APP). A sustained imbalance between production and clearance of Aβ40-42 fragments from APP leads to accumulation of Aβ peptide monomers, oligomers, and finally large aggregated Aβ plaques, which are thought to be able to initiate the pathogenic cascade, ultimately leading to neuronal loss and dementia [6, 7]. Therefore, the inhibition of Aβ aggregation has been considered as the primary therapeutic strategy for the neurodegenerative disease.

Oxidative stress is one of the earliest events in AD pathogenesis [8]. The free radical and oxidative stress theory of aging also suggests that oxidative damage is an important player in neuronal degeneration. Therefore, the successful protection of neuronal cells from oxidative damage could potentially prevent AD. In addition,

dyshomeostasis of metal ions such as Cu, Zn, and Fe ions clearly occur in AD brains [9, 10]. Some studies suggest that the highly concentrated metal ions are able to accelerate the formation of Aβ aggregates and neurofibrillary tangles, which promote inflammation and activate neurotoxic pathways, leading to dysfunction and death of brain cells [11]. Furthermore, the interaction of Aβ with Cu^{2+} contributes to the production of reactive oxygen species (ROS) and oxidative stress which further cause oxidative damage in the brain [12-14]. Therefore, the extent of metal-induced Aβ aggregation and ROS production can be modulated by metal chelators, which highlights metal-ion chelation therapy as a promising AD treatment [15, 16].

Converging lines of evidence support the hypothesis that ligands exhibiting great affinity for the β-amyloid peptide are more effective at preventing amyloid formation and inhibiting amyloid neurotoxicity [17]. Considering the high concentration of Cu^{2+} in amyloid plague, combining metal complexation and ligand interaction may offer a novel method to construct Aβ inhibitors.

Resveratrol (trans-3, 4', 5-trihydroxylstilbene), a phytoalexin with a stilbene structure, is present in medicinal plants, grape skin, peanuts, and red wine. In recent years, resveratrol has been extensively investigated as a cardioprotective, anti-inflammatory, anticancer and anti-aging agent [18-21]. Many studies have shown that resveratrol can counteract Aβ toxicity by its antioxidant properties in cellular models [22], and also can inhibit Aβ aggregation in vitro [23]. ^{18}F-labeled stilbene derivatives have been developed as PET radiotracers for imaging amyloid plagues in the brain, which implies the stilbene structure has a strong affinity to Aβ aggregates [24, 25]. The

metal chelator clioquinol (CQ) has moved into clinical trials and showed improved cognition. Long-term use is, however, limited by an adverse side effect, subacute myelo-optic neuropathy [26]. Although these traditional metal chelators have yet to be available as therapeutic agents, the studies using these compounds show the possible involvement of metal ions in AD pathogenesis [27].

Very recently, our group has reported the synthesis of tacrine–coumarin hybrids as multifunctional cholinesterase inhibitors (ChEIs) against AD [28]. Continuing with our research on various natural products with potential application in the AD field, in this paper, we fashioned small molecules by direct introduction of a metal binding site into the structure of an Aβ aggregate-imaging agent (Figure 1). This approach can afford bifunctional compounds with metal chelating and Aβ interactive activities. The stilbene structure has been chosen as basic structure of bifunctional small molecules because of its properties for the rational structure-based design principle such as strong binding affinity to Aβ species, blood-brain barrier (BBB) penetration, and easy removal from normal brain tissue [29]. For metal chelation, we utilize the Schiff bases and phenolic hydroxyl groups as the chelators. These conjugates are designed to become dimers due to Cu^{2+} coordination, holding great promise for Cu^{2+} elimination and Aβ assembly inhibition abilities.

In this paper, we described the design, synthesis and pharmacological evaluation of a series of imine resveratrol derivatives as multifunctional anti-AD agents. The pharmacological evaluations of these compounds include antioxidant, self-induced Aβ aggregation, ROS induced by Cu-Aβ, metal chelation, and neuroprotection.

2. Result and discussion

2.1. Chemistry

The resveratrol analogues **1**–**20** were synthesized by the classical method of imine formation involving condensation between aromatic amine with a variety of aromatic aldehydes in ethanol under reflux condition (Scheme 1). Imines with (*E*)-configuration were obtained as sole product. Structures of all synthesized compounds were characterized by comparison with ^{1}H and ^{13}C nuclear magnetic resonance (NMR) spectroscopy data reported in the literature.

All synthesized compounds were elucidated by spectroscopic measurements (IR, Mass, ^{1}H NMR and ^{13}C NMR). The IR spectra of titled compounds (**1**–**20**) showed absorption bands of OH stretching vibration at 3410-3455 cm^{-1}. Skelton vibrations for benzene rings appeared in between 1480 and 1590 cm^{-1}. The characteristic strong bands appeared for C=N stretching at 1596–1637 cm^{-1}. In the ^{1}HNMR spectra, aromatic protons appeared as set of multiplet in the region δ 6.24-8.77 ppm and CH=N protons resonated as a singlet between δ 8.52 and 9.63 ppm. Moreover, in the ^{13}C NMR spectra, the carbon resonance frequencies of the CH=N was at δ 157.1–165.2 ppm. The aromatic carbons appeared at δ 103.1–162.9 ppm. Finally, the $-OCH_3$ groups appeared at δ 55.6 ppm.

*2.2. Prediction of BBB penetration of compounds **1**–**20***

A major impediment to development of effective anti-Aβ compounds for AD therapy is that essentially 100% of large-molecule drugs and > 98% of small-molecule drugs fail to cross the BBB [30]. For BBB penetration, molecules should satisfy the

restrictive terms of Lipinski's rules [31]: molecular weight (MW) less than 500, the calculated logarithm of the octanol-water partition coefficient (ClogP) less than 5, the number of hydrogen bond donor atoms (HBD) less than 5, the number of hydrogen bond acceptor atoms (HBA) less than 10, and the small polar surface area less than 90 $Å^2$. Filter for prediction of BBB penetration involves calculation of log BB by means of the equation shown in the footnote of Table 1. Defined by the restrictive terms of Lipinski's rules and calculated log BB for potential applications in brains, compounds **1**–**20** fulfil drug-like criteria and possible brain penetration (Table 1).

2.3. Radical-scavenging activity

DPPH (diphenyl-1-picrylhydrazyl) radicals can be used in preliminary screening of compounds capable of scavenging reactive oxygen species, since these nitrogen radicals are much more stable and easier to handle than oxygen free radicals [32]. For comparison purpose, resveratrol was used as reference compound. The IC_{50} values of all tested compounds were summarized in Table 2. From the Table 2, it could be seen that compounds **1**–**12** had much better scavenging activities compared with resveratrol, while compounds **15** and **20** had lower radical scavenging activities than resveratrol and others had negligible effect on DPPH-scavenging. These results indicated that *ortho*-OH group on A ring was critical in determination of scavenging activity. The most possible reason for this is that the steric effect of the *ortho* hydroxyl radical may be overlapped by the lone electronic pair of the N atom, thus, the lack of electron of hydroxyl radical may be supplemented by the electron from the N atom [33, 34]. From the IC_{50} values of compounds **1–7**, it appeared that *meta*- or *para*-OH

group on B ring had less positive effect than *ortho*-OH, while F atom on B ring had little effect on scavenging activity. IC_{50} values of compounds **13–18** indicated that no matter *meta*- *para*- OH group or F atom on A ring contributed relatively less to the DPPH-scavenging. Replacement of the 3-hydroxyl group on B ring by a methoxy group was found to reduce the ability of scavenging the DPPH free radical. This observation indicated that methoxy group was negative for the activity compared with hydroxyl group. Among the target compounds, compound **9** (IC_{50} = 14.1 μM) bearing *ortho*-OH group on A ring and the *o*-diphenolic group on B ring showed the most potent scavenging activity, which was 7.7 times stronger than that of the reference compound resveratrol (IC_{50} = 108.6 μM). This may due to the stabilization effect of the intramolecular hydrogen bond on resulting *o*-hydroxyphenoxyl radical [34].

2.4. Inhibition of Aβ (1-42) self-induced aggregation

All compounds tested their DPPH radical scavenging activities were also tested for their ability to inhibit A*β* (1-42) self-induced aggregation by using a thioflavin-T based fluorometric assay [35]. Curcumin (Cur) and resveratrol (Res) were used as reference compounds and the results were summarized in Table 2 and showed in Figure 2. From the results, it could be seen that most hybrids exhibited moderate-to-good potencies (24.9 to 71.2 % at 20 μM) compared to those of curcumin (51.5 % at 20 μM) and resveratrol (64.2 % at 20 μM). Noticeably, the optimal A*β* (1-42) aggregation inhibition potency was provided by compound **15** (71.2 % at 20 μM) which featuring a *para*-OH group on the A ring and an *ortho*-OH on the B ring. Compound **9** (64.6 % at 20 μM), which exhibited the most potent radical-scavenging

activity, had a good Aβ aggregation inhibition property. From the inhibition values of compounds **1**–**4**, **8**–**9**, and **13**–**15**, it appeared that introduction of hydroxyl groups into A ring or B ring seemed to be beneficial to Aβ self-induced aggregation inhibitory activity. Inhibition values of compounds **4**, **9**, and **11–12** indicated that the hydroxyl groups were more favorable on the Aβ inhibitory activity than methoxy groups. Surprisingly, introduction of an electron-withdrawing group like F atom on the B ring increased the inhibitory activity while decreased the activity on the A ring.

*2.5. Docking study of **9** with Aβ(1-42)*

To further study the interaction mode of compound **9** for Aβ, molecular docking study was performed using software package MOE 2008.10. The X-ray crystal structure of the protein Aβ(1-42) structure (PDB code 1IYT) [36] used in the docking study was obtained from the Protein Data Bank. As showed in Figure 3, A ring of compound **9** interacted with the phenyl ring of Tyr10 via π-π stacking interaction with the distance of 4.34 Å. A σ-π interaction and a π-π stacking interaction were found between B ring of compound **9** and His6 residue with the distance of 4.12 and 3.86 Å, respectively. These results indicated that the hydrophobic interactions played important roles in the stability of the **9**/Aβ(1-42) complex.

2.6. Metal chelating effect

The chelating effect of all compounds for metals such as Cu^{2+} and Fe^{2+} in methanol was studied by UV–vis spectrometry with wavelength ranging from 200 to 500 nm [37, 38]. In Figure 4a, UV–vis spectra of **9** at increasing Cu^{2+} concentrations were shown as an example. The increase in absorbance, which could be better estimated by

an inspection of the differential spectra (Figure 4b), indicated that there was an interaction between Cu^{2+} and **9**. The similar behavior was also observed when using Fe^{2+}. These observations indicated that our compounds could effectively chelate Cu^{2+} and Fe^{2+}, and thereby could serve as metal chelators in treating AD. The ratio of ligand/metal ion in the complex was investigated by mixing the fix amount metal ion with increasing ligand; it was possible to observe that the maximum intensity of difference spectra was reach at about 1:1 ratio, which was taken as an indication of the stoichiometry of the complex.

2.7. Inhibition of Cu^{2+}-induced Aβ (1-42) aggregation

To investigate the ability of the imine resveratrol derivatives to inhibit Cu^{2+}-induced A*β* (1-42) aggregation, we studied compounds **4**, **6** and **9** by a ThT-binding assay [39]. Resveratrol and clioquinol were used as reference compounds. It could be seen from Figure 5, the fluorescence of A*β* treated with Cu^{2+} is 144.3% that of A*β* alone, which indicates that Cu^{2+} accelerates A*β* aggregation. By contrast, the fluorescence of A*β* treated with Cu^{2+} and the tested compounds decreased dramatically (**4**, 83.7% inhibition of Cu^{2+}-induced A*β* aggregation; **6**, 70.2% inhibition; **9**, 68.1% inhibition; CQ, 66.7% inhibition; Res, 63.4% inhibition). These results suggested that our compounds could inhibit Cu^{2+}-induced A*β* aggregation effectively by chelating Cu^{2+}.

*2.8. Control of Cu-Aβ H_2O_2 production by compound **9***

Binding of redox active metal ions such as Cu^{2+} to A*β* species is known to be involved in generation of ROS such as H_2O_2 and subsequent facilitation of A*β* aggregation and neurotoxicity. The effect of compound **9** on H_2O_2 production by Cu^{2+}-A*β*42 species

was examined using the HRP/Amplex Red assay [40]. Under reducing conditions, the Cu^{2+}-Aβ(1-42) reacted with O_2 to generate H_2O_2. Addition of compound **9** to such a solution reduced the production of H_2O_2 by about 80% for the Cu- Aβ(1-42) species. By comparison, the strong chelator ethylenediaminetetraacetic acid (EDTA) showed an even more pronounced effect, almost complete eliminating (>90%), and clioquinol showed the reducing effect by about 75%. These results presented that compound **9** was able to chelate metal ions as well as regulated ROS production, which showed promise for their further applications (Figure 6).

2.9. Cell viability and neuroprotection studies

To gain insight into the therapeutic potential of these derivatives, cell viability and neuroprotective capacity against oxidative stress were assayed using the human neuroblastoma cell line SH-SY5Y [41]. Compounds **4**, **6** and **9** were selected as representative compounds of different types. First, the colorimetric MTT [3-(4,5-dimethyl-2-thiazolyl)-2,5-diphenyl-2H-tetrazolium bromide] assay was performed to examine the potential cytotoxic effects of compounds **4**, **6** and **9**. As indicated in Figure 7, compounds **4**, **6** and **9** did not show significant effect on cell viability at 1–50 μM after incubation for 24 h. This suggested that compounds **4**, **6** and **9** was nontoxicity to SH-SY5Y cells.

Compounds **4**, **6** and **9** were tested for their capacity to protect human SH-SY5Y neuroblastoma cells against oxidative stress-associated death induced by H_2O_2, and resveratrol was used as the reference compound. In this assay, addition of 100 μM H_2O_2 to the growth medium reduced cell viability to 56.8% compared to control. The

tested compounds were added to the media at different concentration immediately prior to the H_2O_2 insult. Phase-contrast micrographs showed H_2O_2-induced neurotoxicity and neuroprotection in human SH-SY5Y neuroblastoma cells for the tested compounds (Figure 8). From Figure 9, it could be seen that all of the compounds exhibited neuroprotective effects at concentrations ranging from 1.25 to 10 μM. Compound **9** showed higher protective capability much better than resveratrol. Compounds **4** and **6** showed moderate protective capabilities the same as resveratrol at the concentration of 10 μM. These observations further indicated that these new derivatives had the potential to be efficient multifunctional agents, including antioxidant activity, for the treatment of AD.

3. Conclusion

In conclusion, a series of imine resveratrol derivatives were designed and synthesized as multi-targeted agents for the treatment of AD. Among the synthesized compounds, compound **9** exhibited significant inhibition of self-induced and Cu^{2+}-induced Aβ aggregation, antioxidant activity, metal-chelating ability, control of Cu-Aβ H_2O_2 production and low cell toxicity. Furthermore, compound **9** showed neuroprotective capability much better than resveratrol at the concentration of 10 μM. These properties highlighted the potential of these new compounds to be developed as new multifunctional drugs in the treatment of Alzheimer's disease.

4. Experimental section

4.1. Chemistry

All chemicals (reagent grade) used were purchased from Sinopharm Chemical

Reagent Co. , Ltd.(China). Reaction progress was monitored using analytical thin layer chromatography (TLC) on precoated silica gel GF_{254} (Qingdao Haiyang Chemical Plant, Qingdao, China) plates and the spots were detected under UV light (254 nm). Melting point was measured on an XT-4 micromelting point instrument and uncorrected. IR (KBr-disc) spectra were recorded by Bruker Tensor 27 spectrometer. ^{1}H NMR and ^{13}C NMR spectra were measured on a Bruker ACF-500 spectrometer at 25 °C and referenced to TMS. Chemical shifts are reported in ppm (δ) using the residual solvent line as internal standard. Splitting patterns are designed as s, singlet; d, doublet; t, triplet; m, multiplet. The purity of all compounds used for biological evaluation was confirmed to be higher than 95% through analytical HPLC performed with Agilent 1200 HPLC System (Supporting information, Table S1). Mass spectra were obtained on a MS Agilent 1100 Series LC/MSD Trap mass spectrometer (ESI-MS) and a Mariner ESI-TOF spectrometer (HRESIMS), respectively. Column chromatography was performed on silica gel (90-150 μm; Qingdao Marine Chemical Inc.)

*4.1.1.General procedures for the preparation of compounds **1–20***

Compounds **1–20** were easily prepared as described in the literature with some modification [34]. In brief, the mixture of aromatic aldehyde and aniline were stirred in a small amount of ethanol at reflux condition for about 2 h then followed by filtration and recrystallization in EtOAc or MeOH to obtain the pure compounds.

*4.1.1.1. (E)-2-(Benzylideneamino)phenol (**1**)*

Yield 85%, pale white solid, m.p. 88–89 °C; IR (KBr) *v* 2924.32, 2319.87, 1626.93,

1482.50, 1401.37, 1250.65, 1125.20, 1098.78, 764.98, 689.28 cm^{-1}. ^{1}H NMR (500 MHz, $CDCl_3$) δ 8.70 (s, 1H, CH=N), 8.01-7.86 (m, 2H, Ar-H), 7.59-7.42 (m, 3H, Ar-H), 7.36-7.27 (m, 1H, Ar-H), 7.22-7.15 (m, 1H, Ar-H), 7.02 (d, *J* = 8.0 Hz, 1H, Ar-H), 6.95-6.85 (m, 1H, Ar-H). ^{13}C NMR (125 MHz, $CDCl_3$) δ 157.13, 152.38, 135.93, 135.56, 131.68, 128.95, 128.88, 128.82, 120.11, 115.86, 115.04. ESI-MS *m/z*: 198.1 $[M+H]^+$; HRMS: calcd for $C_{13}H_{12}NO$ $[M+H]^+$, 198.0913, found 198.0911.

4.1.1.2. (E)-2-((2-Hydroxybenzylidene)amino)phenol ***(2)***

Yield 78%, red solid, m.p. 191–192 °C; IR (KBr) *v* 2026.29, 1632.31, 1530.02, 1486.68, 1463.01, 1401.52, 1275.86, 1223.37, 1139.51, 764.38, 741.84 cm^{-1}. ^{1}H NMR (500 MHz, DMSO-*d*6) δ 13.77 (s, 1H, OH), 9.71 (s, 1H, OH), 8.96 (s, 1H, CH=N), 7.61 (dd, *J* = 7.7, 1.7 Hz, 1H, Ar-H), 7.41-7.33 (m, 2H, Ar-H), 7.15-7.10 (m, 1H, Ar-H), 6.99-6.91 (m, 3H, Ar-H), 6.88 (td, *J* = 7.6, 1.3 Hz, 1H, Ar-H). ^{13}C NMR (125 MHz, DMSO-*d*6) δ 161.64, 160.63, 150.99, 134.96, 132.72, 132.20, 127.91, 119.57, 119.52, 119.46, 118.63, 116.60, 116.46. ESI-MS *m/z*: 212.1 $[M-H]^-$; HRMS: calcd for $C_{13}H_{10}NO_2$ $[M-H]^-$, 212.0717, found 212.0714.

4.1.1.3. (E)-2-((3-Hydroxybenzylidene)amino)phenol ***(3)***

Yield 75%, dark yellow solid, m.p. 215–216 °C; IR (KBr) *v* 3202.40, 1637.18, 1579.88, 1494.34, 1466.45, 1351.71, 1309.31, 1273.61, 1245.80, 1174.31, 1118.09, 794.23, 733.38 cm^{-1}. ^{1}H NMR (500 MHz, DMSO-*d*6) δ 14.21 (s, 1H, OH), 10.14 (s, 1H, OH), 9.63 (s, 1H, CH=N), 8.77 (s, 1H, Ar-H), 7.37 (d, *J* = 8.5 Hz, 1H, Ar-H), 7.30 (dd, *J* = 8.0, 1.6 Hz, 1H, Ar-H), 7.07 (td, *J* = 7.6, 1.6 Hz, 1H, Ar-H), 6.94 (dd, *J* = 8.0, 1.4 Hz, 1H, Ar-H), 6.85 (td, *J* = 7.6, 1.4 Hz, 1H, Ar-H), 6.35 (dd, *J* = 8.4, 2.2

Hz, 1H, Ar-H), 6.24 (d, *J* = 2.3 Hz, 1H, Ar-H). ^{13}C NMR (125 MHz, DMSO-*d*6) δ 165.23, 162.89, 160.88, 150.95, 135.21, 134.59, 127.50, 120.08, 119.66, 116.85, 112.78, 107.99, 103.14. ESI-MS *m/z*: 212.1 $[M-H]^-$; HRMS: calcd for $C_{13}H_{10}NO_2$ $[M-H]^-$, 212.0717, found 212.0715.

*4.1.1.4. (E)-2-((4-hydroxybenzylidene)amino)phenol (**4**)*

Yield 53%, dark yellow solid, m.p. 163–165 °C; IR (KBr) *v* 2311.09, 1629.83, 1513.49, 1469.62, 1401.43, 1267.91, 1222.44, 1099.40, 765.71, 742.60 cm^{-1}. ^{1}H NMR (500 MHz, DMSO-*d*6): δ 10.13 (s, 1H, OH), 8.81 (s, 1H, OH), 8.54 (s, 1H, CH=N), 7.86 (d, *J* = 8.5 Hz, 2H, Ar-H), 7.13 (dd, *J* = 7.6, 1.2 Hz, 1H, Ar-H), 7.05-7.01 (m, 1H, Ar-H), 6.89-6.86 (m, 3H, Ar-H), 6.82-6.79 (m, 1H, Ar-H). ^{13}C NMR (125 MHz, DMSO-*d*6): δ 161.05, 159.18, 151.51, 138.80, 131.45, 128.31, 127.08, 120.04, 119.17, 116.21, 116.02. ESI-MS *m/z*: 212.1 $[M-H]^-$; HRMS: calcd for $C_{13}H_{10}NO_2$ $[M-H]^-$, 212.0717, found 212.071.

*4.1.1.5. (E)-2-((2-Fluorobenzylidene)amino)phenol (**5**)*

Yield 70%, light yellow solid, m.p. 105 °C; IR (KBr) *v* 2311.29, 1619.78, 1586.13, 1488.44, 1455.19, 1384.28, 1215.37, 1202.92, 1091.32, 763.02, 755.45 cm^{-1}. ^{1}H NMR (500 MHz, DMSO-*d*6) δ 9.14 (s, 1H, OH), 8.90 (s, 1H, CH=N), 8.32 (td, *J* = 7.8, 1.9 Hz, 1H, Ar-H), 7.62-7.53 (m, 1H, Ar-H), 7.38 -7.31 (m, 2H, Ar-H), 7.23 (dd, *J* = 7.8, 1.6 Hz, 1H, Ar-H), 7.14-7.07 (m, 1H, Ar-H), 6.93 (dd, *J* = 8.1, 1.4 Hz, 1H, Ar-H), 6.85 (td, *J* = 7.6, 1.4 Hz, 1H, Ar-H). ^{13}C NMR (125 MHz, DMSO-*d*6) δ 161.57, 152.28, 151.63, 138.24, 133.79, 133.72, 128.68, 128.25, 125.20, 120.22, 120.03,

116.69, 116.33. ESI-MS *m/z*: 216.1 $[M+H]^+$; HRMS: calcd for $C_{13}H_{11}FNO$ $[M+H]^+$, 216.0819, found 216.0817.

*4.1.1.6. (E)-2-((3-Fluorobenzylidene)amino)phenol (**6**)*

Yield 72%, light yellow solid, m.p. 77–78 °C; IR (KBr) *v* 3065.33, 2929.95, 2319.34, 1625.97, 1585.56, 1488.55, 1384.77, 1288.43, 1245.13, 1173.88, 1152.07, 811.78, 786.77, 752.55 cm^{-1}. ^1H NMR (500 MHz, DMSO-*d*6) δ 9.04 (s, 1H, OH), 8.75 (s, 1H, CH=N), 7.96 (ddd, *J* = 10.1, 2.6, 1.3 Hz, 1H, Ar-H), 7.81 (dt, *J* = 7.8, 1.0 Hz, 1H, Ar-H), 7.56 (td, *J* = 8.0, 5.8 Hz, 1H, Ar-H), 7.42-7.31 (m, 1H, Ar-H), 7.25 (dd, *J* = 7.8, 1.6 Hz, 1H, Ar-H), 7.11 (td, *J* = 7.7, 1.6 Hz, 1H, Ar-H), 6.91 (dd, *J* = 8.1, 1.4 Hz, 1H, Ar-H), 6.85 (td, *J* = 7.6, 1.4 Hz, 1H). ^{13}C NMR (125 MHz, DMSO-*d*6) δ 161.97, 158.20, 151.95, 139.41, 137.62, 131.13, 128.36, 126.06, 119.93, 119.47, 118.35, 116.64, 114.69. ESI-MS *m/z*: 216.1 $[M+H]^+$; HRMS: calcd for $C_{13}H_{11}FNO$ $[M+H]^+$, 216.0819, found 216.0819.

*4.1.1.7. (E)-2-((4-Fluorobenzylidene)amino)phenol (**7**)*

Yield 75%, light yellow solid, m.p. 86–88 °C; IR (KBr) *v* 2088.22, 1633.80, 1511.49, 1484.66, 1402.99, 1243.96, 1197.59, 1150.22, 1096.65, 1833.55, 753.72 cm^{-1}. ^1H NMR (500 MHz, $CDCl_3$) δ 8.66 (s, 1H, CH=N), 7.92 (ddd, *J* = 8.6, 5.6, 2.6 Hz, 2H, Ar-H), 7.28 (dd, *J* = 7.9, 2.7 Hz, 1H, Ar-H), 7.19 (qd, *J* = 10.0, 8.8, 5.3 Hz, 4H, Ar-H), 7.02 (dd, *J* = 8.1, 2.7 Hz, 1H, Ar-H), 6.91 (td, *J* = 7.7, 2.5 Hz, 1H, Ar-H). ^{13}C NMR (125 MHz, $CDCl_3$) δ 157.13, 152.38, 135.93, 135.56, 131.68, 128.95, 128.88, 128.82, 120.11, 115.86, 115.04. ESI-MS *m/z*: 216.1 $[M+H]^+$; HRMS: calcd for $C_{13}H_{11}FNO$ $[M+H]^+$, 216.0819, found 216.0820.

*4.1.1.8. (E)-4-(((2-Hydroxyphenyl)imino)methyl)benzene-1,3-diol (**8**)*

Yield 65%, light yellow solid, m.p. 125 °C; IR (KBr) *v* 2923.92, 2026.36, 1627.05, 1589.11, 1455.52, 1401.44, 1384.01, 1247.28, 1124.52, 786.74, 755.93, 683.51, 605.68 cm^{-1}. ^{1}H NMR (500 MHz, DMSO-*d*6) δ 9.63 (s, 1H, OH), 8.97 (s, 1H, OH), 8.59 (s, 1H, CH=N), 7.47-7.37 (m, 2H, Ar-H), 7.30 (t, *J* = 7.8 Hz, 1H, Ar-H), 7.15 (dd, *J* = 7.7, 1.6 Hz, 1H, Ar-H), 7.07 (td, *J* = 7.7, 1.6 Hz, 1H, Ar-H), 6.91 (ddd, *J* = 15.8, 8.0, 1.9 Hz, 2H, Ar-H), 6.82 (td, *J* = 7.6, 1.4 Hz, 1H, Ar-H). ^{13}C NMR (125 MHz, DMSO-*d*6) δ 160.08, 158.09, 151.38, 138.71, 138.23, 130.09, 127.59, 120.77, 119.94, 119.85, 118.96, 116.46, 115.16. ESI-MS *m/z*: 228.1 $[M-H]^-$; HRMS: calcd for $C_{13}H_{10}NO_3$ $[M-H]^-$, 228.0666, found 228.0665.

*4.1.1.9. (E)-4-(((2-Hydroxyphenyl)imino)methyl)benzene-1,2-diol (**9**)*

Yield 55%, red solid, m.p. 188–190 °C; IR (KBr) *v* 3280.68, 2715.09, 2562.30, 1635.81, 1564.80, 1495.10, 1445.20, 1397.83, 1300.99, 1283.82, 1173.21, 1160.54, 804.67, 769.71, 748.84 cm^{-1}. ^{1}H NMR (500 MHz, DMSO-*d*6) δ 9.39 (s, 2H, OH), 8.85 (s, 1H, OH), 8.44 (s, 1H, CH=N), 7.47 (d, *J* = 2.0 Hz, 1H, Ar-H), 7.25 (dd, *J* = 8.3, 2.0 Hz, 1H, Ar-H), 7.10 (dd, *J* = 7.7, 1.6 Hz, 1H, Ar-H), 7.02 (td, *J* = 7.6, 1.6 Hz, 1H, Ar-H), 6.90-6.82 (m, 2H, Ar-H), 6.80 (t, *J* = 7.6 Hz, 1H, Ar-H). ^{13}C NMR (125 MHz, DMSO-*d*6) δ 159.11, 150.71, 149.00, 145.47, 138.59, 128.30, 126.36, 122.35, 119.38, 118.93, 115.61, 115.31, 114.75. ESI-MS *m/z*: 228.1 $[M-H]^-$; HRMS: calcd for $C_{13}H_{10}NO_3$ $[M-H]^-$, 228.0666, found 228.0664.

*4.1.1.10. (E)-2-((4-(Dimethylamino)benzylidene)amino)phenol (**10**)*

Yield 42%, yellow solid, m.p. 121–122 °C; IR (KBr) *v* 2906.70, 2818.38, 1614.68, 1587.91, 1537.52, 1485.03, 1374.95, 1245.54, 1230.85, 1170.60, 1150.57, 811.24, 750.86, 739.60 cm^{-1}. ^{1}H NMR (500 MHz, DMSO-*d*6) δ 8.69 (s, 1H, OH), 8.52 (s, 1H, CH=N), 7.91-7.78 (m, 2H, Ar-H), 7.16 (dd, *J* = 7.9, 1.6 Hz, 1H, Ar-H), 7.03 (td, *J* = 7.7, 1.6 Hz, 1H, Ar-H), 6.87 (dd, *J* = 8.0, 1.4 Hz, 1H, Ar-H), 6.82-6.78 (m, 3H, Ar-H), 3.04 (s, 6H, $N(CH_3)_2$). ^{13}C NMR (125 MHz, DMSO-*d*6) δ 158.49, 152.26, 150.91, 138.50, 131.43, 130.40, 126.10, 124.10, 119.35, 115.38, 111.30, 41.20. ESI-MS *m/z*: 241.1 $[M+H]^+$; HRMS: calcd for $C_{13}H_{10}NO_3$ $[M+H]^+$, 241.1335, found 241.1336.

*4.1.1.11. (E)-2-((4-Methoxybenzylidene)amino)phenol (**11**)*

Yield 60%, yellow solid, m.p. 90–92 °C; IR (KBr) *v* 2969.79, 2925.81, 2319,65, 1596.17, 1569.21, 1511,14, 1484.53, 1383.84, 1257.52, 1167.80, 1108.39, 1027.25, 833.61, 756.38 cm^{-1}. ^{1}H NMR (500 MHz, DMSO-*d*6) δ 8.85 (s, 1H, OH), 8.62 (s, 1H, CH=N), 8.01-7.93 (m, 2H, Ar-H), 7.19-7.14 (m, 1H, Ar-H), 7.05 (dd, *J* = 8.1, 6.4 Hz, 3H, Ar-H), 6.89 (d, *J* = 7.9 Hz, 1H, Ar-H), 6.82 (t, *J* = 7.5 Hz, 1H, Ar-H), 3.84 (s, 3H, OCH_3). ^{13}C NMR (125 MHz, DMSO-*d*6) δ 162.63, 156.81, 152.23, 136.10, 130.68, 129.02, 128.37, 120.22, 115.96, 114.40, 55.58. ESI-MS *m/z*: 228.1 $[M+H]^+$; HRMS: calcd for $C_{14}H_{13}NO_2$ $[M+H]^+$, 228.0860, found 228.0861.

*4.1.1.12. (E)-2-((3,4-Dimethoxybenzylidene)amino)phenol (**12**)*

Yield 71%, yellow solid, m.p. 106–108 °C; IR (KBr) *v* 2970.45, 1623.12, 1582.23, 1514.99, 1463.57, 1383.87, 1279.52, 1242.92, 1139.70, 1016.97, 875.69, 807.78, 756.04 cm^{-1}. ^{1}H NMR (500 MHz, DMSO-*d*6) δ 8.87 (s, 1H, OH), 8.60 (s, 1H, CH=N), 7.76 (d, J = 1.7 Hz, 1H, Ar-H), 7.46 (dd, *J* = 8.2, 1.7 Hz, 1H, Ar-H), 7.19 (dd, *J* = 7.8,

1.3 Hz, 1H, Ar-H), 7.11-7.02 (m, 2H, Ar-H), 6.89 (dd, *J* = 8.0, 1.0 Hz, 1H, Ar-H), 6.85-6.78 (m, 1H, Ar-H), 3.86 (s, 3H, OCH_3), 3.84 (s, 3H, OCH_3). ^{13}C NMR (125 MHz, DMSO-*d*6) δ 158.49, 151.69, 151.09, 149.00, 137.85, 129.40, 126.86, 124.14, 119.37, 118.52, 115.73, 111.13, 109.95, 55.58, 55.57. ESI-MS m/z: 258.1 $[M+H]^+$; HRMS: calcd for $C_{15}H_{16}NO_3$ $[M+H]^+$, 258.1125, found 258.1124.

*4.1.1.13. (E)-2-((Phenylimino)methyl)phenol (**13**)*

Yield 82%, light yellow solid, m.p. 51 °C; IR (KBr) *v* 2978.37, 2321.77, 1617.48, 1588.49, 1482.94, 1452.89, 1384.93, 1275.75, 1186.20, 1149.35, 1074.20, 896.63, 780.61, 755.31, 691.42 cm^{-1}. ^1H NMR (500 MHz, DMSO-*d*6) δ 13.09 (s, 1H, OH), 8.96 (s, 1H, CH=N), 7.67 (dd, *J* = 7.7, 1.7 Hz, 1H, Ar-H), 7.47 (dd, *J* = 8.3, 7.1 Hz, 2H, Ar-H), 7.43 (td, *J* = 7.9, 1.6 Hz, 3H, Ar-H), 7.32 (td, *J* = 7.2, 1.4 Hz, 1H, Ar-H), 7.03-6.95 (m, 2H, Ar-H). ^{13}C NMR (125 MHz, DMSO-*d*6) δ 163.96, 160.77, 148.61, 133.74, 133.03, 129.92, 127.40, 121.82, 119.80, 119.60, 117.07. ESI-MS *m/z*: 198.1 $[M+H]^+$; HRMS: calcd for $C_{13}H_{12}NO$ $[M+H]^+$, 198.0913, found 198.0912.

*4.1.1.14. (E)-2-(((3-Hydroxyphenyl)imino)methyl)phenol (**14**)*

Yield 61%, light yellow solid, m.p. 124–128 °C; IR (KBr) *v* 2974.71, 1625.05, 1455.49, 1384.51, 1287.54, 1232.01, 1084.59, 844.01, 756.15, 678.32 cm^{-1}. ^1H NMR (500 MHz, DMSO-*d*6) δ 13.12 (s, 1H, OH), 9.64 (s, 1H, OH), 8.91 (s, 1H, CH=N), 7.65 (dd, *J* = 7.6, 1.7 Hz, 1H, Ar-H), 7.41 (ddd, *J* = 8.7, 7.4, 1.7 Hz, 1H, Ar-H), 7.25 (t, *J* = 8.0 Hz, 1H, Ar-H), 7.02-6.91 (m, 2H, Ar-H), 6.87-6.81 (m, 1H, Ar-H), 6.78 (t, *J* = 2.2 Hz, 1H, Ar-H), 6.73 (dd, *J* = 8.0, 2.3 Hz, 1H, Ar-H). ^{13}C NMR (125 MHz, DMSO-*d*6) δ 163.60, 160.79, 158.80, 149.79, 133.67, 133.02, 130.63, 119.75, 119.56,

117.04, 114.56, 112.51, 108.62. ESI-MS *m/z*: 212.1 $[M-H]^-$; HRMS: calcd for $C_{13}H_{10}NO_2$ $[M-H]^-$, 212.0717, found 212.0709.

*4.1.1.15. (E)-2-(((4-Hydroxyphenyl)imino)methyl)phenol (**15**)*

Yield 68%, dark yellow solid, m.p. 141–142 °C; IR (KBr) *v* 1619.97, 1508.96, 1457.97, 1401.35, 1259.16, 1210.92, 1186.40, 1151.29, 1107.17, 838.28, 801.78, 754.56 cm^{-1}. ^1H NMR (500 MHz, DMSO-*d*6) δ 13.43 (s, 1H, OH), 9.67 (s, 1H, OH), 8.90 (s, 1H, CH=N), 7.59 (dd, *J* = 7.7, 1.7 Hz, 1H, Ar-H), 7.37 (ddd, *J* = 8.7, 7.3, 1.7 Hz, 1H, Ar-H), 7.35-7.29 (m, 2H, Ar-H), 7.08-6.90 (m, 2H, Ar-H), 6.88-6.77 (m, 2H, Ar-H).^{13}C NMR (125 MHz, DMSO-*d*6) δ 160.65, 160.63, 157.44, 139.73, 132.97, 132.65, 123.09, 119.94, 119.43, 116.93, 116.45. ESI-MS *m/z*: 212.1 $[M-H]^-$; HRMS: calcd for $C_{13}H_{10}NO_2$ $[M-H]^-$, 212.0717, found 212.0712.

*4.1.1.16. (E)-2-(((2-Fluorophenyl)imino)methyl)phenol (**16**)*

Yield 60%, yellow solid, m.p. 67–68 °C; IR (KBr) *v* 2028.16, 1626.82, 1493.38, 1403.33, 1285.67, 1230.97, 1199.50, 1180.90, 1127.19, 1106.79, 808.92, 755.93 cm^{-1}. ^1H NMR (500 MHz, DMSO-*d*6) δ 13.00 (s, 1H, OH), 9.05 (s, 1H, CH=N), 7.69 (dd, *J* = 7.6, 1.7 Hz, 1H, Ar-H), 7.60 (dd, *J* = 8.7, 7.3 Hz, 1H, Ar-H), 7.46 (ddd, *J* = 8.7, 7.4, 1.7 Hz, 1H, Ar-H), 7.39-7.33 (m, 2H, Ar-H), 7.32-7.27 (m, 1H, Ar-H), 7.01 (ddd, *J* = 10.1, 7.8, 1.9 Hz, 2H, Ar-H). ^{13}C NMR (125 MHz, DMSO-*d*6) δ 165.31, 160.89, 156.84, 154.87, 136.46, 134.20, 133.07, 128.82, 125.62, 121.30, 119.70, 117.22, 116.87. ESI-MS *m/z*: 216.1 $[M+H]^+$; HRMS: calcd for $C_{13}H_{11}FNO$ $[M+H]^+$, 216.0819, found 216.0817.

*4.1.1.17. (E)-2-(((3-Fluorophenyl)imino)methyl)phenol (**17**)*

Yield 64%, yellow solid, m.p. 45–46 °C; IR (KBr) *v* 2369.65, 2026.35, 1625.17, 1604.21, 1499.40, 1461.38, 1402.34, 1372.47, 1282.57, 1220.11, 1128.39, 824.68, 756.22, 679.47 cm^{-1}. ^{1}H NMR (500 MHz, DMSO-*d*6) δ 12.73 (s, 1H, OH), 8.98 (s, 1H, CH=N), 7.67 (dd, *J* = 7.7, 1.7 Hz, 1H, Ar-H), 7.54-7.41 (m, 2H, Ar-H), 7.33 (dt, *J* = 10.6, 2.3 Hz, 1H, Ar-H), 7.26 (ddd, *J* = 7.9, 1.8, 0.8 Hz, 1H, Ar-H), 7.15 (td, *J* = 8.5, 2.5 Hz, 1H, Ar-H), 7.04-6.94 (m, 2H, Ar-H). ^{13}C NMR (125 MHz, DMSO-*d*6) δ 165.04, 164.22, 162.28, 160.72, 150.82, 134.11, 133.10, 131.51, 119.72, 118.53, 117.13, 113.81, 108.75. ESI-MS *m/z*: 216.1 $[M+H]^+$; HRMS: calcd for $C_{13}H_{11}FNO$ $[M+H]^+$, 216.0819, found 216.0818.

*4.1.1.18. (E)-2-(((4-Fluorophenyl)imino)methyl)phenol (**18**)*

Yield 60%, light yellow solid, m.p. 82–83 °C; IR (KBr) *v* 2975.88, 2349.28, 1621.29, 1503.50, 1458.48, 1384.58, 1272.68, 1230.89, 1181.90, 1150.05, 1078.54, 838.88, 755.12 cm^{-1}. ^{1}H NMR (500 MHz, DMSO-*d*6) δ 12.93 (s, 1H, OH), 8.94 (s, 1H, CH=N), 7.65 (dd, *J* = 7.6, 1.7 Hz, 1H, Ar-H), 7.52-7.45 (m, 2H, Ar-H), 7.42 (ddd, *J* = 8.6, 7.4, 1.7 Hz, 1H, Ar-H), 7.34-7.25 (m, 2H, Ar-H), 7.03-6.94 (m, 2H, Ar-H). ^{13}C NMR (125 MHz, DMSO-*d*6) δ 163.87, 162.41, 160.64, 160.48, 145.11, 133.74, 132.98, 123.73, 119.63, 117.07, 116.70, 116.52. ESI-MS *m/z*: 216.1 $[M+H]^+$; HRMS: calcd for $C_{13}H_{11}FNO$ $[M+H]^+$, 216.0819, found 216.0810.

*4.1.1.19. (E)-4-Chloro-2-((phenylimino)methyl)phenol (**19**)*

Yield 75%, dark yellow solid, m.p. 109–110 °C; IR (KBr) *v* 2349.58, 2316.95, 1618.82, 1564.21, 1483.81, 1400.17, 1355.80, 1276.35, 1183.38, 1123.54, 1094.92, 810.25, 763.65 cm^{-1}. ^{1}H NMR (500 MHz, DMSO-*d*6) δ 13.03 (s, 1H, OH), 8.94 (s,

1H, CH=N), 7.76 (d, *J* = 2.7 Hz, 1H, Ar-H), 7.51-7.46 (m, 2H, Ar-H), 7.45 (dd, *J* = 8.8, 2.7 Hz, 1H, Ar-H), 7.43-7.39 (m, 2H, Ar-H), 7.37-7.31 (m, 1H, Ar-H), 7.01 (d, *J* = 8.8 Hz, 1H, Ar-H). ^{13}C NMR (125 MHz, DMSO-*d*6) δ 162.43, 159.41, 148.41, 133.19, 131.49, 129.96, 127.71, 123.04, 121.86, 121.09, 119.10. ESI-MS *m/z*: 230.0 $[M-H]^-$; HRMS: calcd for $C_{13}H_9ClNO$ $[M-H]^-$, 230.0378, found 230.0376.

*4.1.1.20. (E)-4-Methoxy-2-((phenylimino)methyl)phenol (**20**)*

Yield 70%, dark yellow solid, m.p. 56 °C; IR (KBr) *v* 3057.90, 2935.30, 2830.87, 2026.07, 1622.43, 1577.20, 1494.98, 1399.85, 1276.14, 1210.63, 1183.95, 1156.10, 1046.62, 797.10, 760.77, 681.36 cm^{-1}. ^{1}H NMR (500 MHz, DMSO-*d*6) δ 12.42 (s, 1H, OH), 8.92 (s, 1H, CH=N), 7.49-7.45 (m, 2H, Ar-H), 7.41-7.38 (m, 2H, Ar-H), 7.34-7.30 (m, 1H, Ar-H), 7.26 (d, *J* = 3.1 Hz, 1H, Ar-H), 7.05 (dd, *J* = 8.9, 3.1 Hz, 1H, Ar-H), 6.91 (d, *J* = 8.9 Hz, 1H, Ar-H), 3.76 (s, 3H, OCH_3). ^{13}C NMR (125 MHz, DMSO-*d*6) δ 163.48, 154.82, 152.40, 148.89, 129.92, 127.34, 121.76, 120.98, 119.70, 117.93, 115.75, 56.10. ESI-MS *m/z*: 226.1 $[M-H]^-$; HRMS: calcd for $C_{14}H_{12}NO_2$ $[M-H]^-$, 226.0674, found 226.0670.

4.2. DPPH free radical-scavenging assay

DPPH was used to assess free radical-scavenging activity [32, 34]. DPPH is one of the few stable and commercially available organic nitrogen radicals and has a UV–vis absorption maximum at 517 nm. Upon reduction, the solution color fades; the reaction progress is conveniently monitored by a spectrophotometer. To test free radical-scavenging effects, compounds **1–20** were adjusted with methanol solution to final concentrations of 0–200 μM. Methanolic DPPH (400 μM) was used in the

reaction mixture. Serial dilutions of the test sample (20 μL) were combined with the DPPH (180 μL, 400 μM) solution in a 96-well microtitre plate. MeOH was used as a negative control and resveratrol was used as a positive control. The reaction mixtures were incubated for 30 min at 37 ℃ in the dark and the change in absorbance at 517 nm was measured. Mean values were obtained from triplicate experiments. Inhibition percent was calculated using the equation: DPPH radical-scavenging rate (%) = [1- (A - C) / B] × 100, where A is the absorbance of the sample (DPPH + compounds), B is the absorbance of the DPPH radical-methanol solution, and C is the absorbance of the sample (compounds) alone. Percent inhibition was plotted against concentration, and the equation for the line was used to obtain the IC_{50} value. The IC_{50} values of samples were compared against the standard, resveratrol, and the lower the IC_{50} of synthesized compounds, the better it is as an antioxidant.

4.3. Inhibition of Aβ (1-42) self-induced aggregation

Inhibition of A*β* (1-42) aggregation was measured using a Thioflavin T (ThT)-binding assay [35]. HFIP pretreated A*β* (1-42) samples (Anaspec Inc) were resolubilized with a 50 mM phosphate buffer (pH 7.4) to give a 25 μM solution. Each tested compound was firstly prepared in DMSO at a concentration of 10 mM and 1 μL of each was added to the well of black, opaque Corning 96-well plates such that the final solvent concentration was 10%.The final concentration of each compound was 20 μM and was prepared in independent triplicates. The solvent control was also included. Then, 9 μL of 25 μM A*β* (1-42) sample was added to each well and the samples mixed by gentle trapping. Plates were covered to minimize evaporation and incubated in dark at

room temperature for 46–48 h with no agitation. After the incubation period, 200 μL of 5 μM ThT in 50 mM glycine-NaOH buffer (pH 8.0) was added to each well. Fluorescence was measured on a SpectraMax M5 (Molecular Devices, Sunnyvale, CA, USA) multi-mode plate reader with excitation and emission wavelengths at 446 nm and 490 nm, respectively. The fluorescence intensities were compared and the percent inhibition due to the presence of the inhibitor was calculated by the following formula: $100-(IF_i/IF_o \times 100)$ where IF_i and IF_o are the fluorescence intensities obtained for Aβ (1-42) in the presence and in the absence of inhibitor, respectively.

4.4. Docking study

Molecular modeling calculations and docking studies were performed using Molecular Operating Environment (MOE) software version 2008.10 (Chemical Computing Group, Montreal, Canada). The X-ray crystal structure of Aβ(1-42) (PDB 1IYT) used in the docking study was obtained from the Protein Data Bank (www.rcsb.org). Heteroatoms and water molecules in the PDB file were removed at the beginning, and all hydrogen atoms were added to the protein. Amber99 force field was assigned to the enzyme and the partial charges were calculated with the same force field. Protonate states of the enzyme at pH 7 was obtained by following the Protonate 3D protocol in which all configurations were set as default. Compound **9** was drawn in MOE with all hydrogen atoms added. During the docking procedure, pose of compound **9** was initially generated by Triangle Matcher method, and scored with london dG function. 30 Poses of the compound were dedicated to the next refinement procedure. All poses were fine tune with the force field refinement scheme.

The best 10 poses of molecules were retained and scored. After docking, the geometry of resulting complex was studied using the MOE's pose viewer utility.

4.5. Spectrophotometric measurement of complex with Cu^{2+} and Fe^{2+}

The study of metal chelation was performed in methanol at 298 K using UV–vis spectrophotometer (SHIMADZU UV-2450PC) with wavelength ranging from 200 to 500 nm [37, 38]. The difference UV–vis spectra due to complex formation was obtained by numerical subtraction of the spectra of the metal alone and the compound alone (at the same concentration used in the mixture) from the spectra of the mixture. A fixed amount of **9** (25 μmol/L) was mixed with growing amounts of copper ion (2–50 μmol/L) and tested the difference UV–vis spectra to investigate the ratio of ligand/metal in the complex.

4.6. Inhibition of Cu^{2+}-induced Aβ (1-42) aggregation

For the inhibition of Cu^{2+}-induced Aβ (1-42) aggregation experiment [39], the Aβ was diluted in 20 μM HEPES (pH 6.6) with 150 μM NaCl. The mixture of the peptide (10 μL, 25 μM, final concentration) with or without copper (10μL, 25 μM, final concentration) and the test compound (10 μL, 50 μM, final concentration) was incubated at 37 °C for 24 h. The 20 μL of the sample was diluted to a final volume of 200 μL with 50 mM glycine-NaOH buffer (pH 8.0) containing thioflavin T (5 μM). The detection method was the same as that of self-induced Aβ aggregation experiment.

4.7. Hydrogen Peroxide Assays

Hydrogen peroxide production was determined using a HRP/Amplex Red assay. A

general protocol from Invitrogen's Amplex Red Hydrogen Peroxide/Peroxidase Assay as followed [40]. Reagents were added directed to a 96-well plate in the following order to give a 100 μL final solution: $CuCl_2$ (400 nM), phosphate buffer, Aβ peptide (200 μM), compounds (800 nM, 1% v/v DMSO), and sodium ascorbate (10 μM). The reaction was allowed to incubate for 30 min at room temperature. After this incubation, 50 μM of freshly prepared working solution containing 100 nM Amplex Red (Sigma) and 0.2 U/mL HRP (Sigma) in phosphate buffer was added to each well, and the reaction was allowed to incubate for 30 min at room temperature. Fluorescence was measured using a SpectraMax Paradigm plate reader ($\lambda_{ex}/_{em}$ = 530/590). Error bars represent standard deviations for at least three measurements.

4.8. Cell culture and MTT assay for cell viability

The SH-SY5Y cells were cultured in Eagle's minimum essential medium (EMEM)/ ham's F-12 (1:1) medium supplemented with 10% fetal bovine serum (FBS), 100 U/mL penicillin and 100 μg/mL streptomycin, at 37 ℃ in a humidified atmosphere containing 5% CO_2. Cells were subcultured in 96-well plates at a seeding density of 1 × 10^4 cells/well and allowed to adhere and grow. When cells reached the required confluence, they were placed into serum-free medium and treated with compounds **4**, **6** and **9**. Twenty-four hours later the survival of cells was determined by MTT assay. Briefly, after incubation with 20 μL of MTT at 37 ℃ for 4 h, living cells containing MTT formazan crystals were solubilized in 200 μL DMSO. The absorbance of each well was measured using a microculture plate reader with a test wavelength of 570 nm and a reference wavelength of 630 nm. Results are expressed as the mean ± SD of

three independent experiments.

4.9. Neuroprotection activity in SH-SY5Y cells

SH-SY5Y cells were seeded at 1×10^4 cells/well in 96-well plates. After 24 h, the medium was removed and replaced with the tested compounds (1.25, 2.5, 5, 10 μM) at 37 °C and incubated for another 24 h. Resveratrol was used as the control with concentration of 10 μM. Then, the cells were exposed to H_2O_2 (100 μM) and incubated at 37 °C for 24h before assayed with MTT [41]. Results are expressed as percent viability compared to untreated cells for three independent experiments.

Acknowledgments

This research work was financially supported by Innovative Research Team in University (IRT1193), A Project Funded by the Priority Academic Program Development of Jiangsu Higher Education Institutions (PAPD), Project of Graduate Education Innovation of Jiangsu Province (No. CXZZ13_0320).

References

[1] M. Goedert, M.G. Spillantini, Science 314 (2006) 777-781.

[2] E. Scarpini, P. Scheltens, H. Feldman, Lancet. Neurol. 2 (2003) 539-547.

[3] V. Tumiatti, A. Minarini, M.L. Bolognesi, A. Milelli, M. Rosini, C. Melchiorre, Curr. Med. Chem. 17 (2010) 1825-1838.

[4] H.W. Querfurth, F.M. LaFerla, N. Engl. J. Med. 362 (2010) 329-344.

[5] M. Jucker, L.C. Walker, Ann. Neurol. 70 (2011) 532-540.

[6] J. Hardy, D.J. Selkoe, Science 297 (2002) 353-356.

[7] Y. Suzuki, J.R. Brender, M.T. Soper, J. Krishnamoorthy, Y. Zhou, B.T. Ruotolo, N.A. Kotov, A. Ramamoorthy, E.N. Marsh, Biochemistry 52 (2013) 1903-1912.

[8] D.J. Bonda, X. Wang, G. Perry, A. Nunomura, M. Tabaton, X. Zhu, M.A. Smith, Neuropharmacology 59 (2010) 290-294.

[9] C. Opazo, X. Huang, R.A. Cherny, R.D. Moir, A.E. Roher, A.R. White, R. Cappai, C.L. Masters, R.E. Tanzi, N.C. Inestrosa, A.I. Bush, J. Biol. Chem. 277 (2002) 40302-40308.

[10] P. Zatta, D. Drago, S. Bolognin, S.L. Sensi, Trends Pharmacol. Sci. 30 (2009) 346-355.

[11] J. Dong, C.S. Atwood, V.E. Anderson, S.L. Siedlak, M.A. Smith, G. Perry, P.R. Carey, Biochemistry 42 (2003) 2768-2773.

[12] X. Huang, R.D. Moir, R.E. Tanzi, A.I. Bush, J.T. Rogers, Ann. N. Y. Acad. Sci. 1012 (2004) 153-163.

[13] F. Gu, M. Zhu, J. Shi, Y. Hu, Z. Zhao, Neurosci. Lett. 440 (2008) 44-48.

[14] D.A. Butterfield, A.M. Swomley, R. Sultana, Antioxid. Redox Signal. (2013).

[15] H.P. Lee, G. Casadesus, X. Zhu, H.G. Lee, G. Perry, M.A. Smith, K. Gustaw-Rothenberg, A. Lerner, Expert Rev. Neurother. 9 (2009) 1615-1621.

[16] A.I. Bush, J. Alzheimers Dis. 15 (2008) 223-240.

[17] C.W. Cairo, A. Strzelec, R.M. Murphy, L.L. Kiessling, Biochemistry 41 (2002) 8620-8629.

[18] S. Pervaiz, Drug Resist Updat. 7 (2004) 333-344.

[19] J.A. Baur, D.A. Sinclair, Nat. Rev. Drug Discov. 5 (2006) 493-506.

[20] R. Csuk, S. Albert, B. Siewert, S. Schwarz, Eur. J. Med. Chem. 54 (2012) 669-678.

[21] V.P. Androutsopoulos, K.C. Ruparelia, A. Papakyriakou, H. Filippakis, A.M. Tsatsakis, D.A. Spandidos, Eur. J. Med. Chem. 46 (2011) 2586-2595.

[22] J.H. Jang, Y.J. Surh, Free Radic. Biol. Med. 34 (2003) 1100-1110.

[23] M. Narasimhulu, T. Srikanth Reddy, K. Chinni Mahesh, A. Sai Krishna, J. Venkateswara Rao, Y. Venkateswarlu, Bioorg. Med. Chem. Lett. 19 (2009) 3125-3127.

[24] W. Zhang, S. Oya, M.P. Kung, C. Hou, D.L. Maier, H.F. Kung, J. Med. Chem. 48 (2005) 5980-5988.

[25] I. Lee, Y.S. Choe, J.Y. Choi, K.H. Lee, B.T. Kim, J. Med. Chem. 55 (2012) 883-892.

[26] E.R. Vardy, I. Hussain, N.M. Hooper, Expert Rev. Neurother. 6 (2006) 695-704.

[27] J.S. Choi, J.J. Braymer, R.P. Nanga, Proc. Natl. Acad. Sci. USA 107 (2010) 21990-21995.

[28] S.S. Xie, X.B. Wang, J.Y. Li, L. Yang, L.Y. Kong, Design, Eur. J. Med. Chem. 64 (2013) 540-553.

[29] H.F. Kung, C.W. Lee, Z.P. Zhuang, M.P. Kung, C. Hou, K. Plossl, J. Am. Chem. Soc. 123 (2001) 12740-12741.

[30] W.M. Pardridge, Alzheimers Dement. 5 (2009) 427-432.

[31] J.J. Braymer, A.S. Detoma, J.S. Choi, K.S. Ko, M.H. Lim, Int. J. Alzheimers Dis.

2011 (2010) 623051.

[32] J.C. Jung, E. Lim, Y. Lee, J.M. Kang, H. Kim, S. Jang, S. Oh, M. Jung, Eur. J. Med. Chem. 44 (2009) 3166-3174.

[33] ZQ. Liu, QSAR Comb. Sci. 26 (2007) 488-495.

[34] J. Lu, C. Li, Y.F. Chai, D.Y. Yang, C.R. Sun, Bioorg. Med. Chem. Lett. 22 (2012) 5744-5747.

[35] M. Bartolini, C. Bertucci, M.L. Bolognesi, A. Cavalli, C. Melchiorre, V. Andrisano, Chembiochem 8 (2007) 2152-2161.

[36] C. Yang, X. Zhu, J. Li, R. Shi, J. Mol. Model. 16 (2010) 813-821.

[37] W. Huang, D. Lv, H. Yu, R. Sheng, S.C. Kim, P. Wu, K. Luo, J. Li, Y. Hu, Bioorg. Med. Chem. 18 (2010) 5610-5615.

[38] R. Joseph, B. Ramanujam, A. Acharya, A. Khutia, C.P. Rao, J. Org. Chem. 73 (2008) 5745-5758.

[39] C. Lu, Y. Guo, J. Yan, Z. Luo, H.B. Luo, M. Yan, L. Huang, X. Li, J. Med. Chem. 56 (2013) 5843–5859.

[40] R.A. Himes, G.Y. Park, G.S. Siluvai, N.J. Blackburn, K.D. Karlin, Angew. Chem. Int. Ed. Engl. 47 (2008) 9084-9087.

[41] H. Zheng, M.B. Youdim, M. Fridkin, J. Med. Chem. 52 (2009) 4095-4098.

Figure and scheme Captions

Figure 1. Combination of the main features of resveratrol and clioquinol provides molecules with multifunctionality (metal chelation, Aβ interaction, and antioxidant).

Figure 2. Inhibition of Aβ (1-42) self-induced aggregation by compounds (**1**-**20**) comparing with those of curcumin (Cur) and resveratrol (Res). The thioflavin-T fluorescence method was used and the measurements were carried out in the presence of 20 μM test compound. The mean ± SD values from three independent experiments were shown.

Figure 3. Docking study of **9** (colored blue) with Aβ(1-42) (PDB code 1IYT). (a) Cartoon representations of **9** interacting with Aβ(1-42). (b) Association of **9** (colored blue) and the Aβ(1-42) obtained from docking calculations. The interactions between the ligand and residue Tyr10 and His6 are indicated by the green line.

Figure 4. (a) Uv–vis (200–500 nm) absorption spectra of compound **9** (25 μM) in methanol after addition of ascending amounts of $CuCl_2$ (2–50 μmol/L). (b) The differential spectra due to **9**-Cu^{2+} complex formation obtained by numerical subtraction from the above spectra of those of Cu^{2+} and **9** at the corresponding concentrations.

Figure 5. Inhibition of Cu^{2+}-induced Aβ (1-42) aggregation by compounds **4**, **6** and **9**

comparing with those of resveratrol (Res) and clioquinol (CQ) ([Aβ = 25 μM, [**4**] = 50 μM, [**6**] = 50 μM, [**9**] = 50 μM, [Res] = 50 μM, [CQ] = 50 μM, [Cu^{2+}] = 25 μM, 37 °C, 24 h). Values are reported as the mean ± SD of three independent experiments. *p<0.05, **p< 0.01.

Figure 6. Production of H_2O_2 from reactions of Aβ, Cu^{2+}, and compound upon addition of ascorbate, as determined by a HRP/Amplex-Red assay. Lanes: (1) Aβ; (2) Aβ + Cu^{2+}; (3) Aβ + Cu^{2+} + **9**; (4) Aβ + Cu^{2+} + CQ; (5) Aβ + Cu^{2+} + EDTA ([Aβ] = 200 nM, [Cu^{2+}] = 400 nM, [chelator] = 800 nM, [ascorbate] = 10 μM, [Amplex Red] = 50 nM, [HRP] = 0.1 U/mL, and $\lambda_{ex/em}$ = 530/590 nm). Values are reported as the mean ± SD of three independent experiments.

Figure 7. Effects of compounds on cell viability in SH-SY5Y cells. The cell viability was determined by the MTT assay after 24 h of incubation with various concentrations of **4**, **6** and **9**. The results were expressed as a percentage of control cells. Values are reported as the mean ± SD of three independent experiments.

Figure 8. Phase-contrast micrographs showing H_2O_2-induced neurotoxicity and neuroprotection of compound **9** in SH-SY5Y cells. (A) Cells without compound treatment showed healthy shapes. (B) Compound **9** (50 μM) alone did not induce neurotoxicity. (C) H_2O_2 alone (100 μM) induced neurotoxicity. (D) Compound **9** (10 μM) was given for 24 h with H_2O_2 (100 μM) at 37 °C and co-treatment showed

neuroprotection (original magnification, 200).

Figure 9. Neuroprotection against H_2O_2 toxicity. Compounds **4**, **6** and **9** were tested for neuroprotective activity against H_2O_2 toxicity in SH-SY5Y neuroblastoma cell cultures. Resveratrol (10 μM) was used as the reference compound. Results are expressed as percent viability compared to cells not treated with H_2O_2. Data represent the mean ± SD of three observations. $^{###}p<0.001$, $*p<0.05$, $**p< 0.01$.

Scheme 1. Structure scheme of imine resveratrol analogues and chemical structure of compounds investigated.

Table 1. Physical properties of compounds **1-20**.

Compounds	MW[a]	ClogP[a]	HBA[a]	HBD[a]	PSA[a]	log BB[a]
1	197.23	1.662	2	1	32.138	-0.093
2	213.23	2.417	3	2	52.954	-0.286
3	213.23	2.417	3	2	52.954	-0.286
4	213.23	2.417	3	2	52.954	-0.286
5	215.22	2.326	2	1	32.138	0.008
6	215.22	2.326	2	1	32.138	0.008
7	215.22	2.326	2	1	32.138	0.008
8	229.23	2.021	4	3	73.769	-0.655
9	229.23	2.021	4	3	73.769	-0.655
10	240.31	2.866	3	1	35.491	0.040
11	227.26	2.527	3	1	41.068	-0.094
12	257.28	2.283	4	1	49.999	-0.263
13	197.23	3.084	2	1	32.138	0.123
14	213.23	2.417	3	2	52.954	-0.286
15	213.23	2.417	3	2	52.954	-0.286
16	215.22	3.398	2	1	32.138	0.171
17	215.22	3.398	2	1	32.138	0.171
18	215.22	3.398	2	1	32.138	0.171
19	231.68	3.901	2	1	32.138	0.247
20	227.26	3.194	3	1	41.068	0.008
rules	$\leqslant$450	$\leqslant$5.0	$\leqslant$10	$\leqslant$5	$\leqslant$90	$\geqslant$-1.0

[a] MW: molecular weight. ClogP: calculated logarithm of the octanol-water partition coefficient. HBA: hydrogen-bond acceptor atoms, HBD: hydrogen-bond donor atoms. PSA: polar surface area. log BB = -0.0148×PSA + 0.152×ClogP + 0.130.

Table 2. DPPH scavenging activities and inhibition of Aβ (1-42) self-induced aggregation of imine resveratrol analogues.

	IC_{50} (μM)	
Compounds	DPPH scavenging activities [a]	Aβ(1-42) aggregation inhibition (%)[b]
1	39.9 ± 7.5	51.7 ± 2.7
2	51.8 ± 3.5	67.2 ± 2.1
3	66.6 ± 4.9	64.3 ± 2.3
4	26.5 ± 3.8	70.9 ± 1.8
5	43.9 ± 3.7	69.4 ± 1.4
6	36.8 ± 2.4	67.6 ± 1.8
7	41.3 ± 1.4	67.8 ± 1.3
8	37.8 ± 2.8	63.1 ± 1.6
9	14.1 ± 0.9	64.6 ± 1.2
10	45.1 ± 1.2	55.8 ± 0.8
11	32.7 ± 2.4	35.7 ± 1.4
12	28.5 ± 1.7	39.4 ± 0.7
13	>2000	44.9 ± 1.7
14	>2000	66.1 ± 1.0
15	398.7 ± 5.6	71.2 ± 0.8
16	>2000	27.8 ± 1.3
17	>2000	31.3 ± 1.7
18	>2000	24.9 ± 0.4
19	>2000	33.8 ± 1.1
20	794.4 ± 4.8	29.0 ± 0.8
Resveratrol[c]	108.6 ± 4.2	64.2 ± 2.1
Curcumin[c]	—	51.5 ± 1.8

[a] IC_{50} values were expressed as mean ± SD for three determinations.

[b] Inhibition of Aβ (1–42) self-induced aggregation, the thioflavin-T fluorescence method was used, the mean ± SD of at least three independent experiments and the measurements were carried out in the presence of 20 μM compounds.

[c] Resveratrol and curcumin were used as positive control.

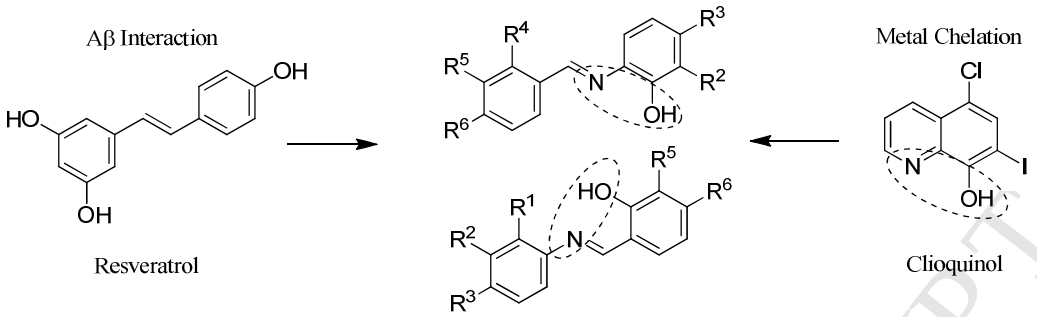

Figure 1

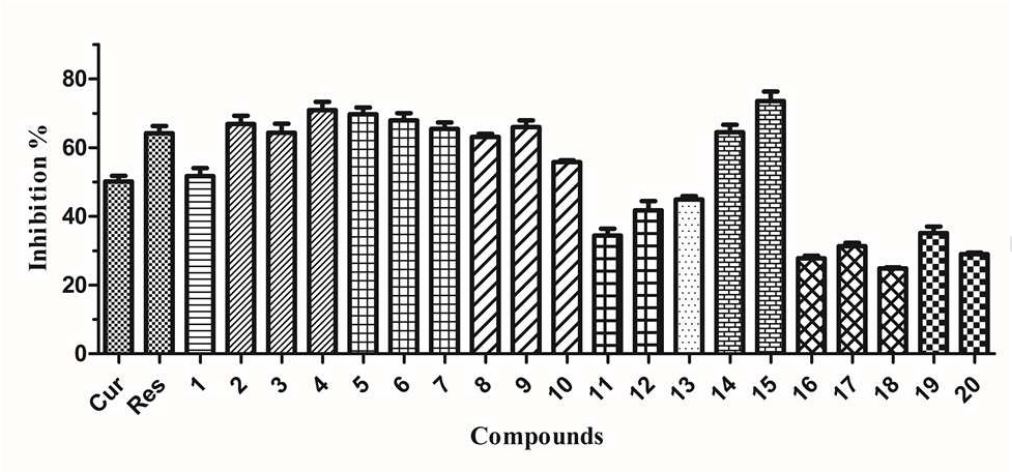

Figure 2

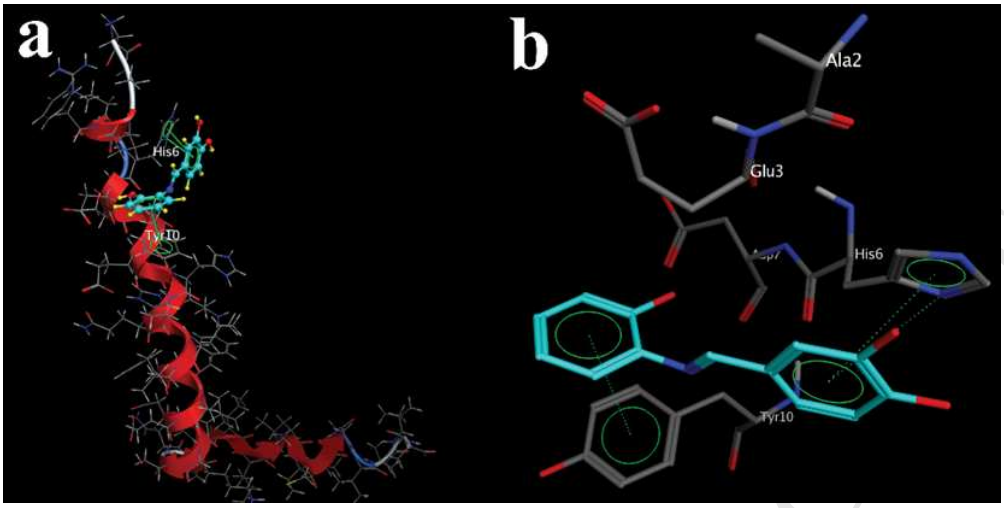

Figure 3

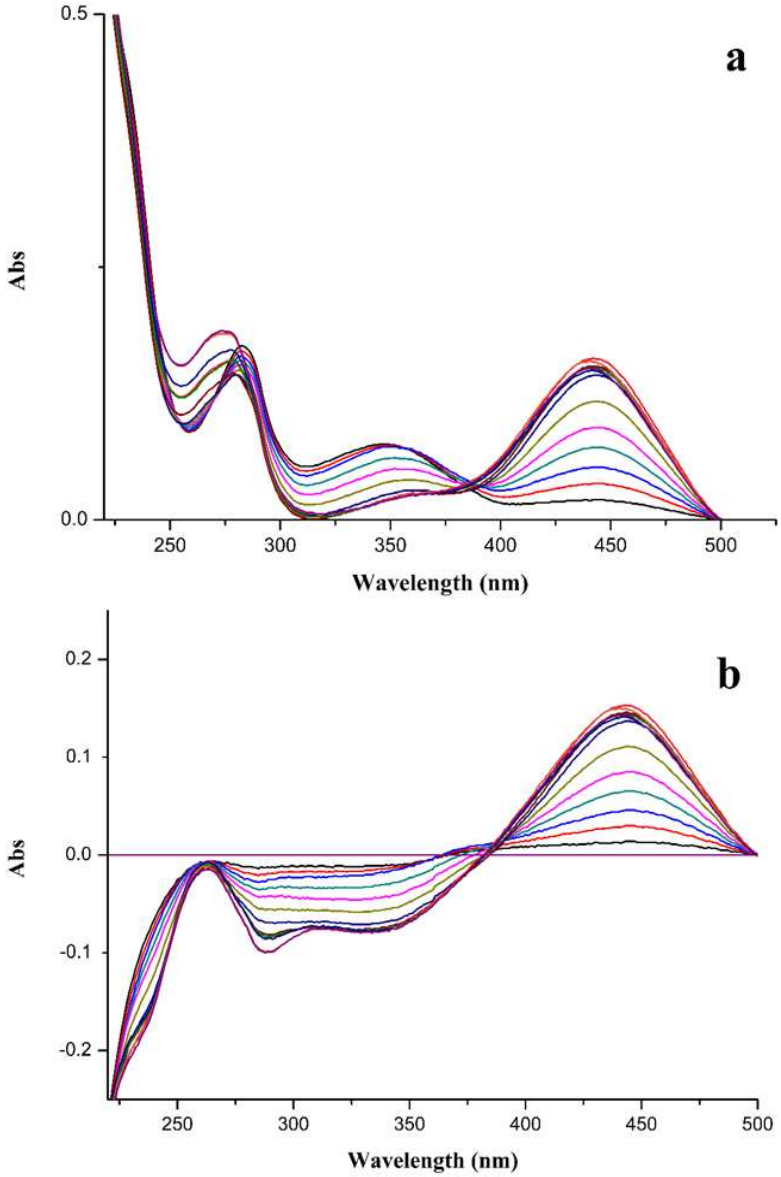
a
Abs
0.5
0.0
250
300
350
400
450
500
Wavelength (nm)
b
Abs
0.2
0.1
0.0
-0.1
-0.2
250
300
350
400
450
500
Wavelength (nm)

Figure 4

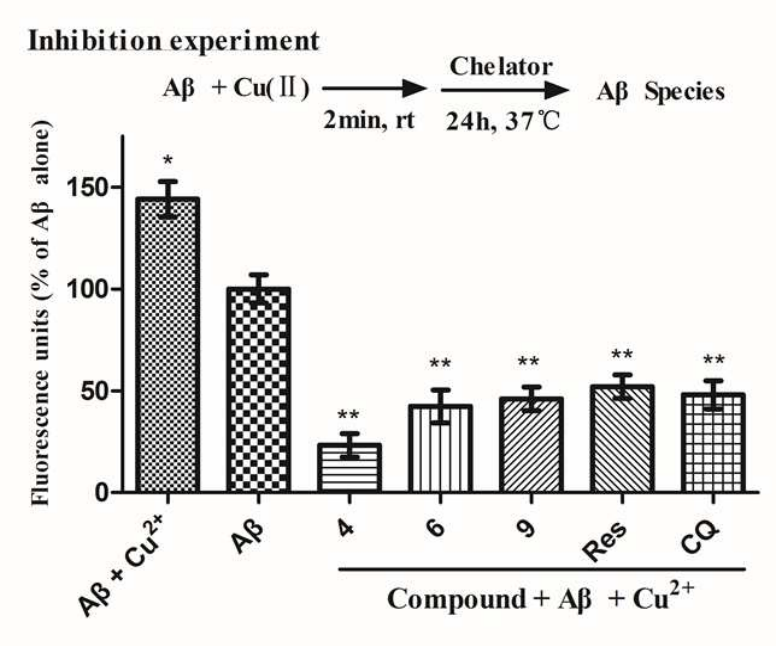

Figure 5

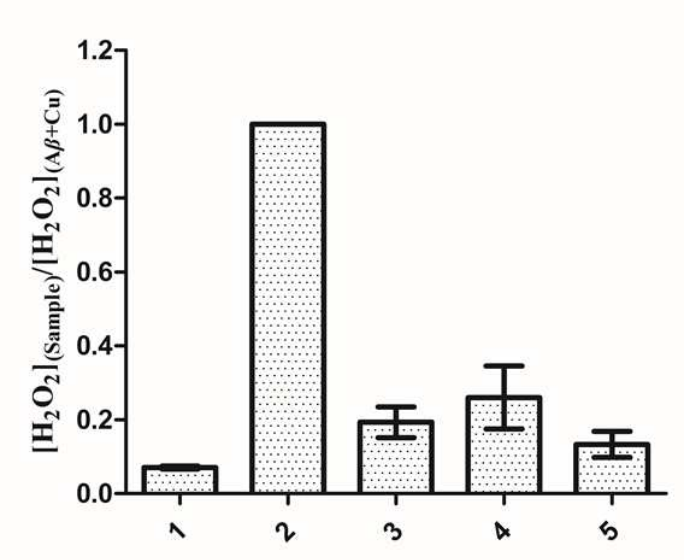

Figure 6

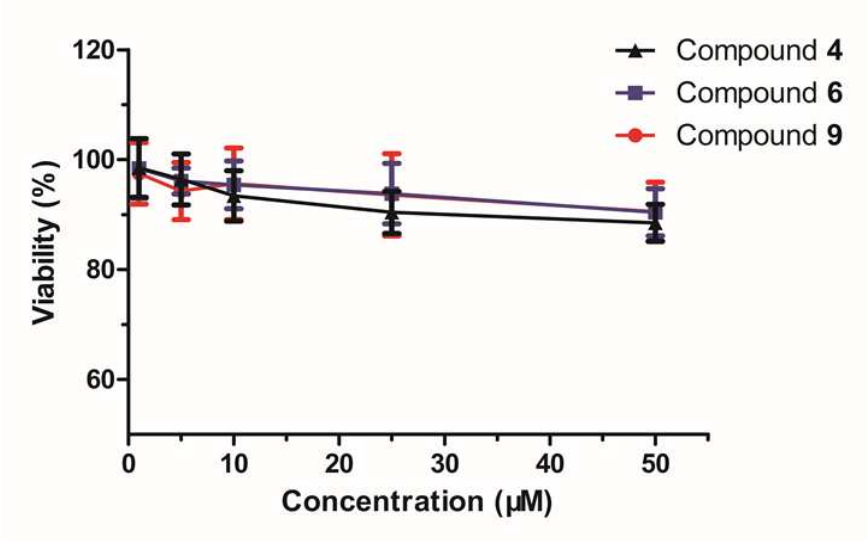

Figure 7

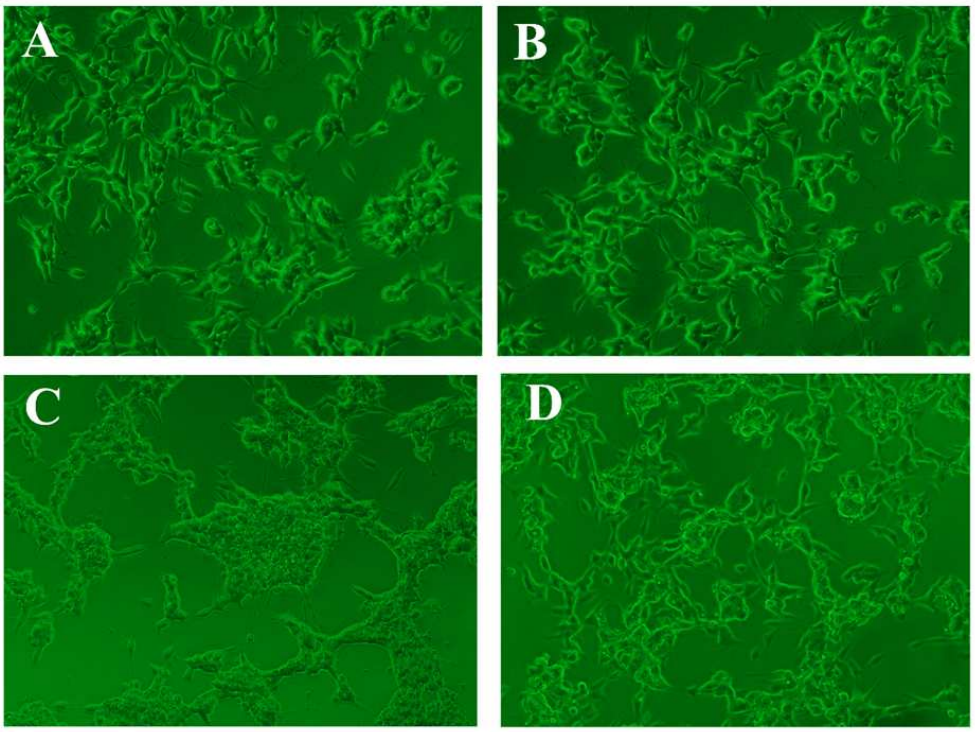

Figure 8

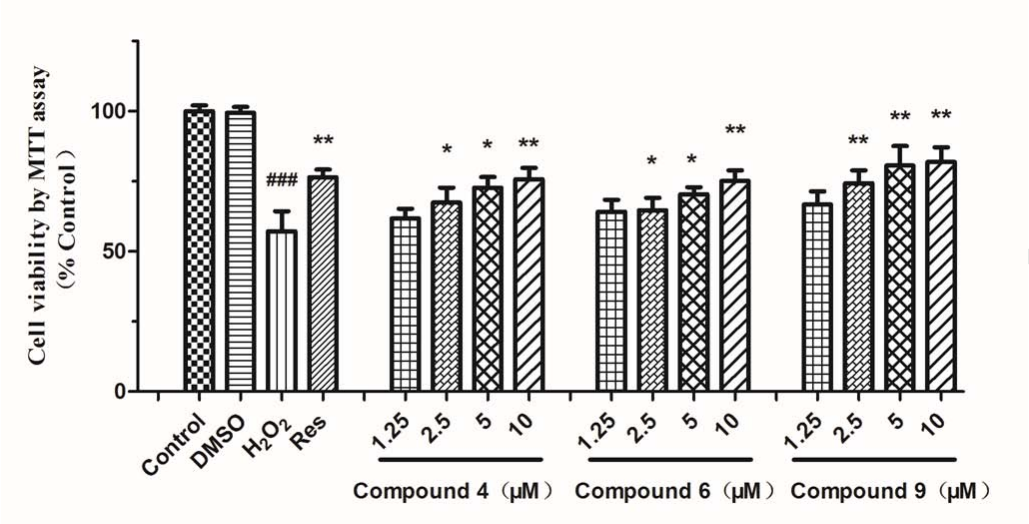

Figure 9

Scheme 1

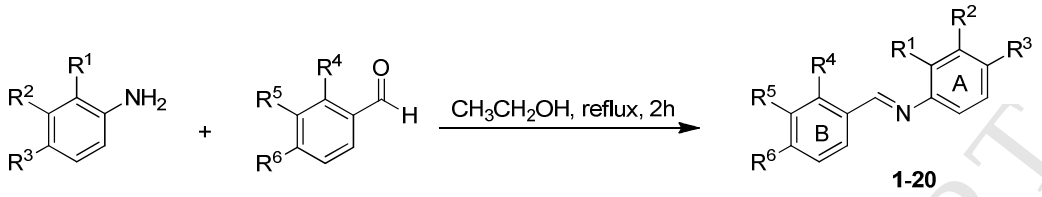

Compound	R^1	R^2	R^3	R^4	R^5	R^6
1	OH	H	H	H	H	H
2	OH	H	H	OH	H	H
3	OH	H	H	H	OH	H
4	OH	H	H	H	H	OH
5	OH	H	H	F	H	H
6	OH	H	H	H	F	H
7	OH	H	H	H	H	F
8	OH	H	H	OH	H	OH
9	OH	H	H	H	OH	OH
10	OH	H	H	H	H	$N(CH_3)_2$
11	OH	H	H	H	H	OCH_3
12	OH	H	H	H	OCH_3	OCH_3
13	H	H	H	OH	H	H
14	H	OH	H	OH	H	H
15	H	H	OH	OH	H	H
16	F	H	H	OH	H	H
17	H	F	H	OH	H	H
18	H	H	F	OH	H	H
19	H	H	H	OH	H	Cl
20	H	H	H	OH	H	OCH_3

Highlights

- A series of imine resveratrol derivatives (**1**-**20**) were designed and synthesized.
- Most of the compounds could function as antioxidants and inhibit Aβ aggregation.
- Most of the compounds showed neuroprotection and metal chelating ability.
- **9** was found to be a promising lead compound for further study.

Design, synthesis and biological evaluation of imine resveratrol derivatives as multi-targeted agents against Alzheimer's disease

Su-Yi Li, Xiao-Bing Wang, Ling-Yi Kong *

State Key Laboratory of Natural Medicines, Department of Natural Medicinal Chemistry, China Pharmaceutical University, 24 Tong Jia Xiang, Nanjing 210009, People's Republic of China

* *Corresponding Author. Tel/Fax: +86-25-83271405; E-mail: cpu_lykong@126.com (Ling-Yi Kong);*

Contents

The representative ^{1}H NMR, ^{13}C NMR spectra, IR spectra and HRMS spectra of compounds.

^{1}H NMR of compound **1** in $CDCl_3$

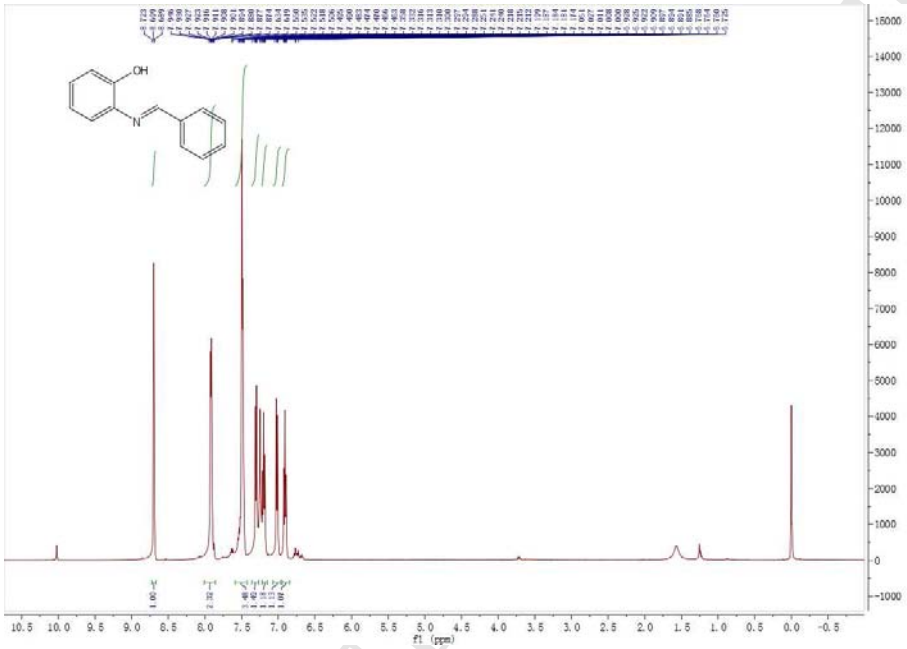

^{13}C NMR of compound **1** in $CDCl_3$

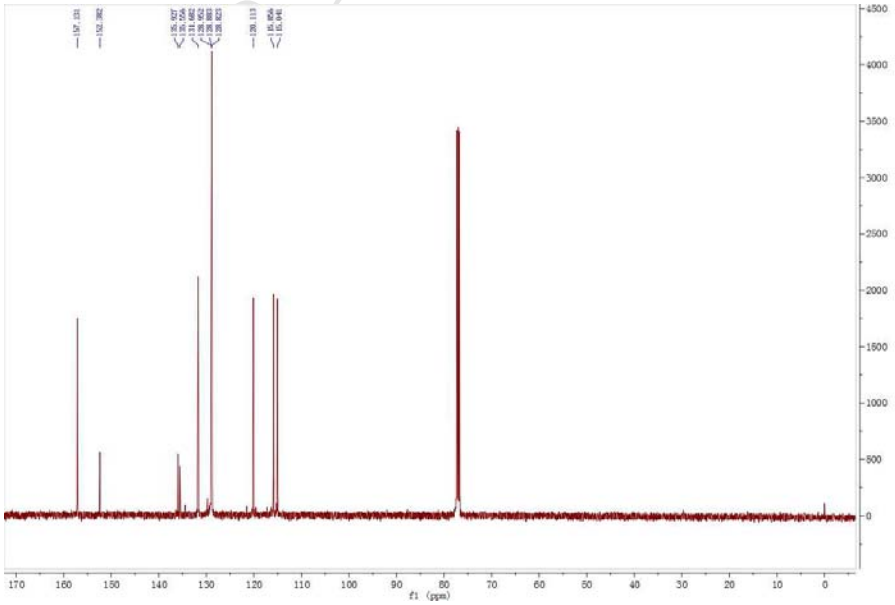

IR of compound **1**

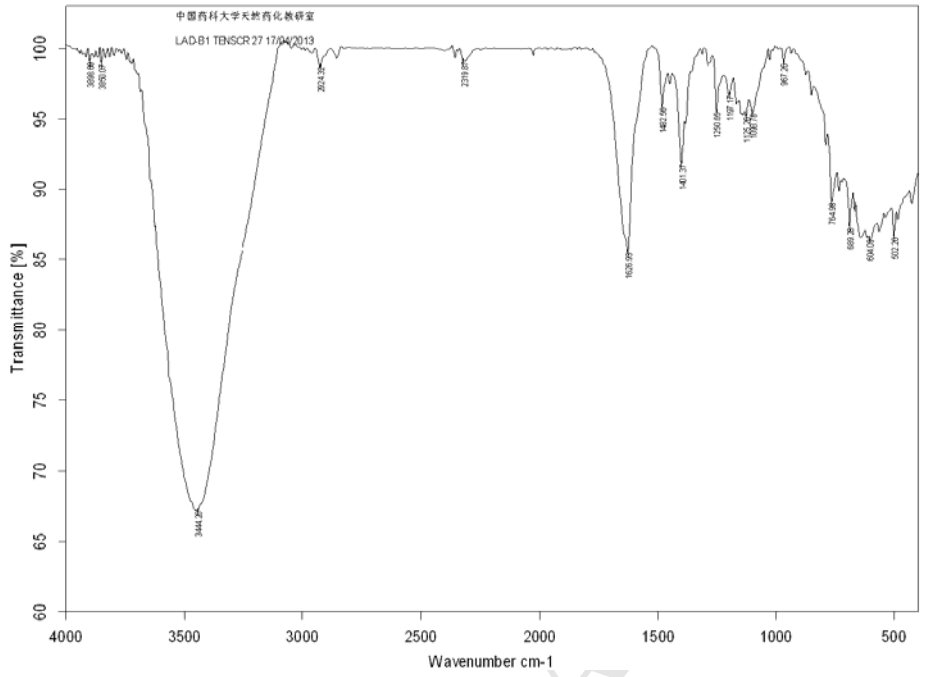

HRMS of compound **1**

TCM-CPU HR-ESI-MS Display Report

Sample Name: Lad-B1 **Instrument:** Agilent 6520B Q-TOF

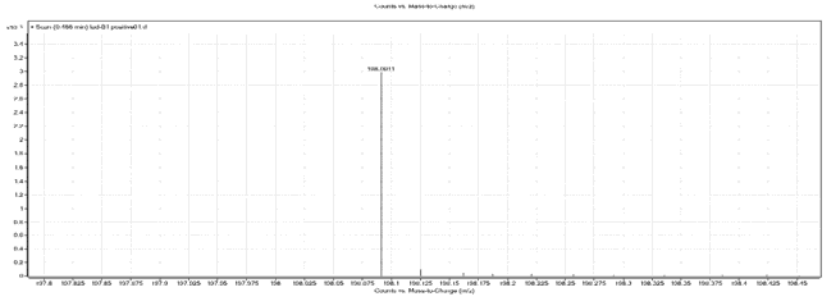

Elemental Composition Calculator

Target m/z:	198.0911	**Result type:**	Positive ions	**Species:**	$[M+H]^+$
Elements:		C (0-80); H (0-120); O (0-30); N(0-10); Na (0-5); F(0-5)			
Ion Formula		**Calculated m/z**		**PPM Error**	
C13H12NO		198.0913		1.04	

Agilent Technologies

^{1}H NMR of compound **3** in DMSO-*d*6

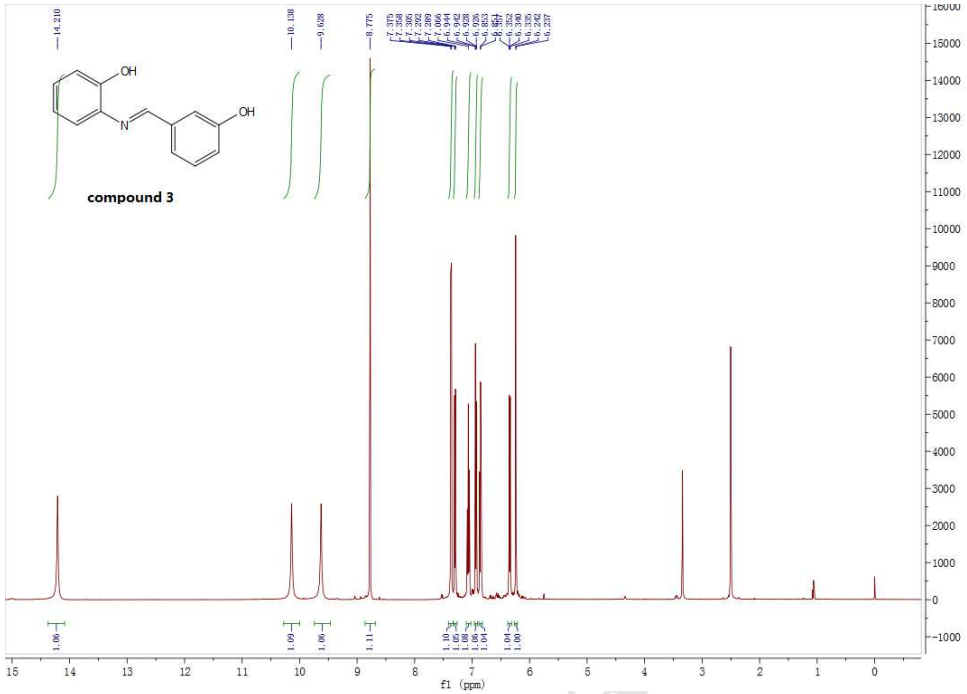

^{13}C NMR of compound **3** in DMSO-*d*6

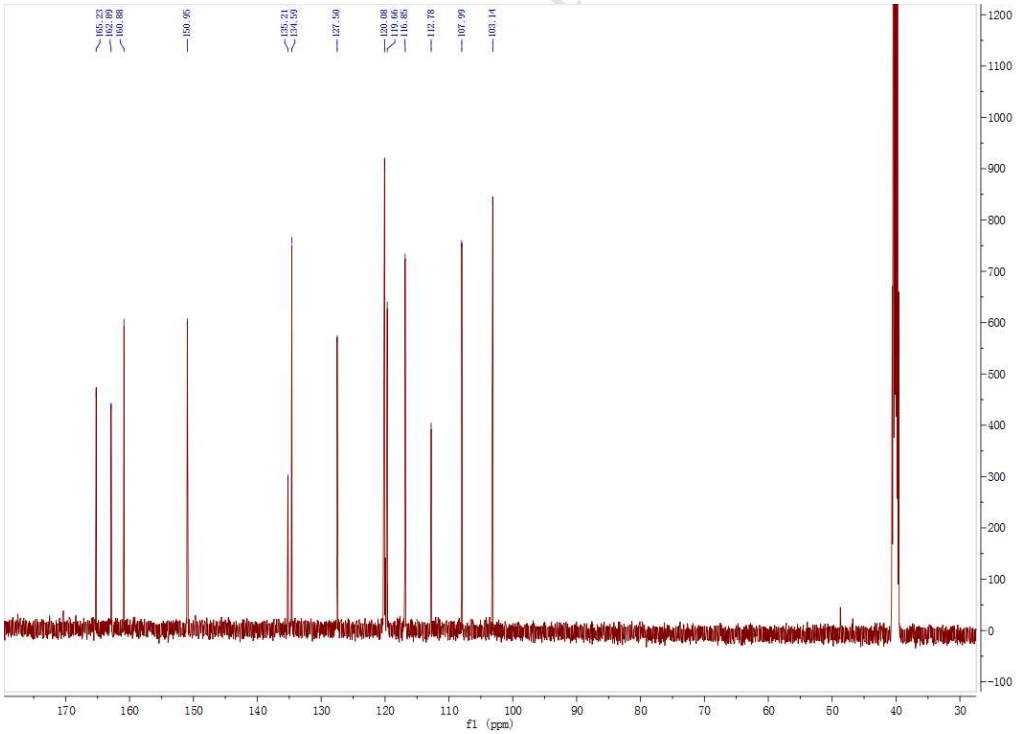

IR of compound **3**

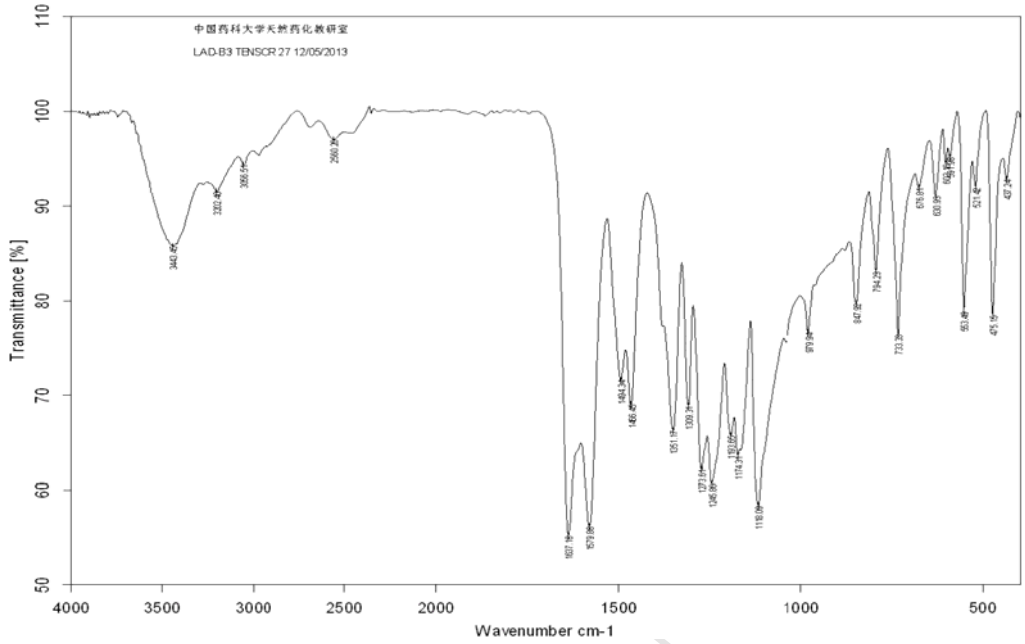

HRMS of compound **3**

TCM-CPU HR-ESI-MS Display Report

Sample Name: Lad-B3 **Instrument:** Agilent 6520B Q-TOF

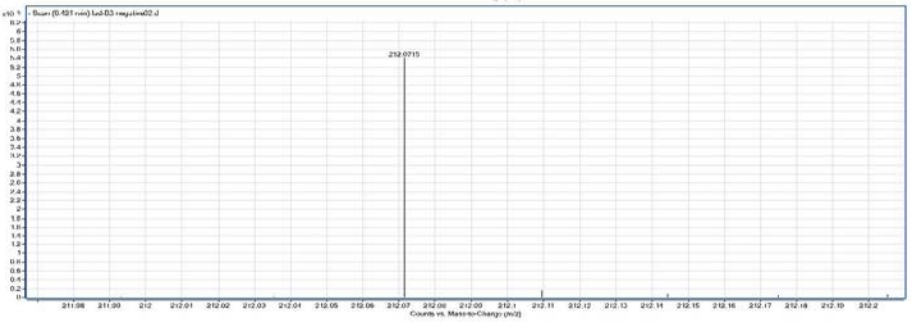

Elemental Composition Calculator

Target m/z:	212.0715	**Result type:**	Negative ions	**Species:**	$[M-H]^-$
Elements:		C (0-80); H (0-120); O (0-30); N(0-10); S(0-5); Cl (0-5)			
Ion Formula		**Calculated m/z**		**PPM Error**	
C13H10NO2		212.0717		1.09	

Agilent Technologies

^{1}H NMR of compound **7** in $CDCl_3$

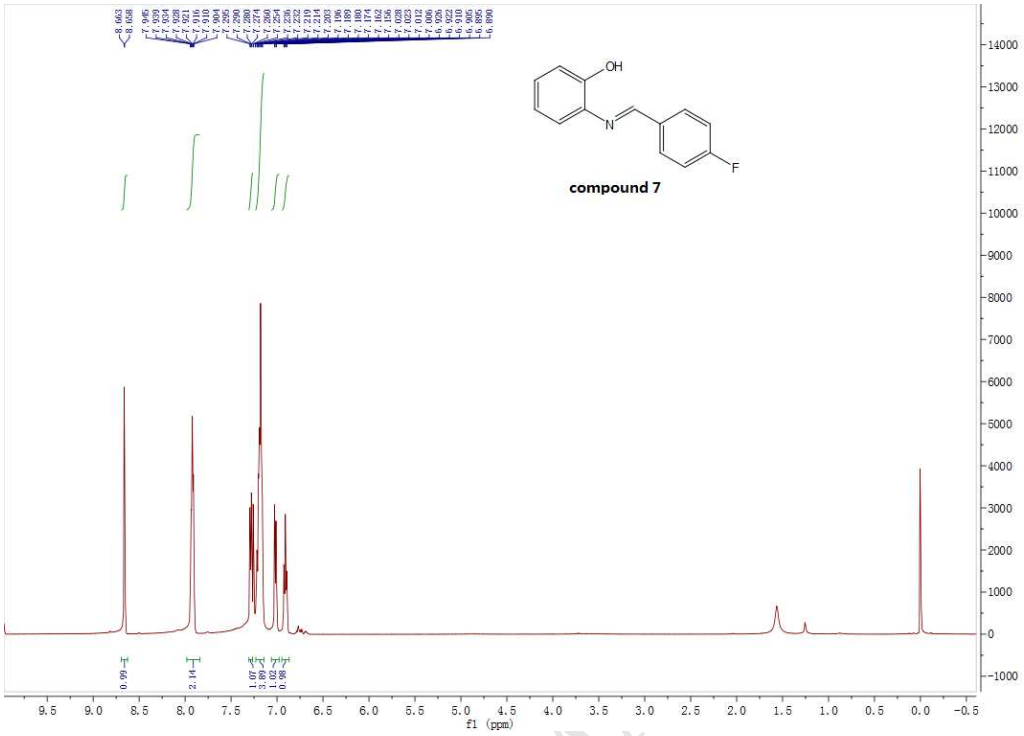

^{13}C NMR of compound **7** in $CDCl_3$

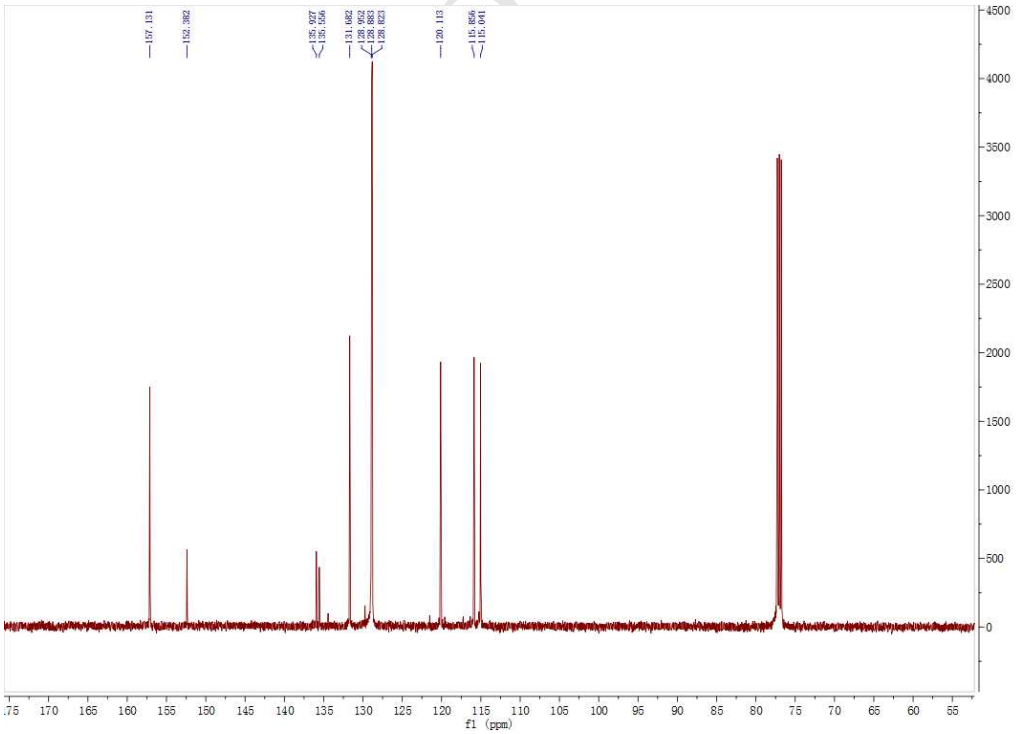

IR of compound **7**

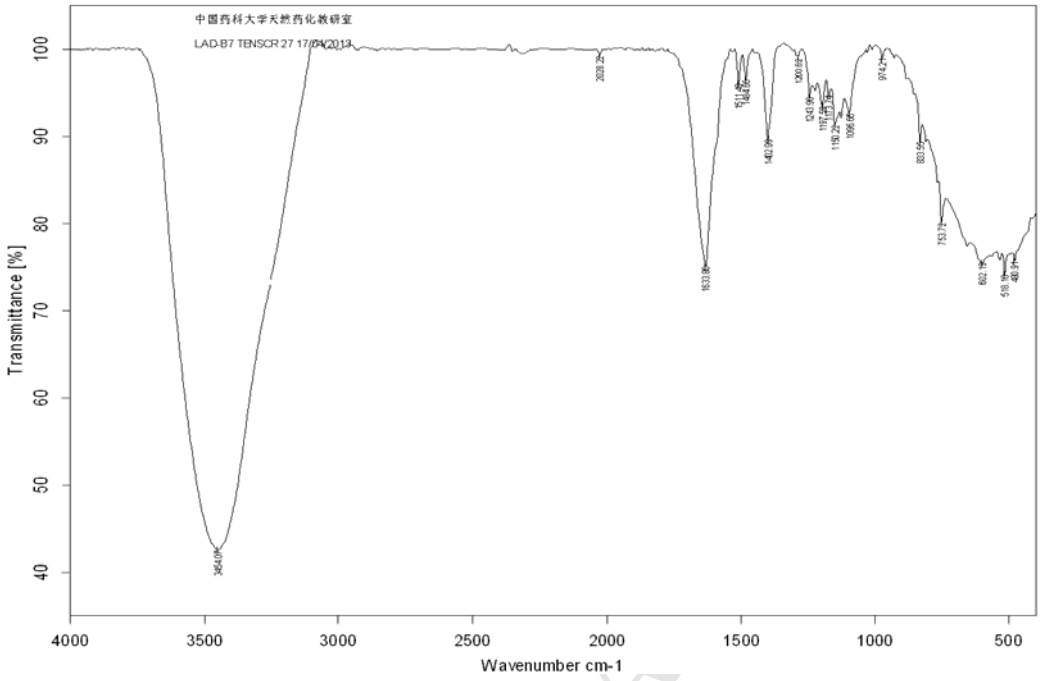

HRMS of compound **7**

TCM-CPU HR-ESI-MS Display Report

Sample Name: Lad-B7 **Instrument:** Agilent 6520B Q-TOF

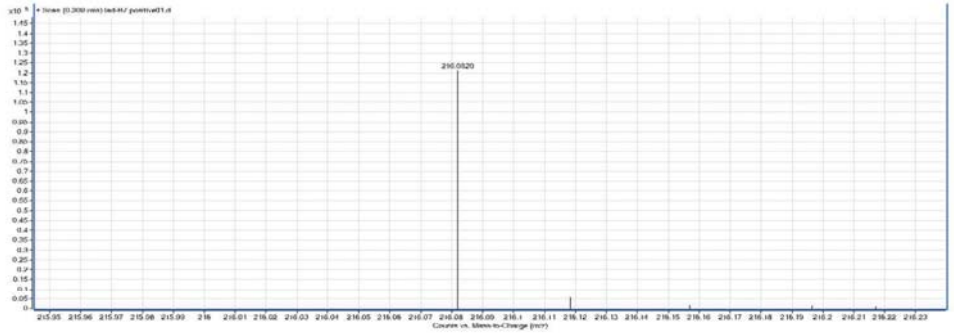

Elemental Composition Calculator

Target m/z:	216.0820	**Result type:**	Positive ions	**Species:**	$[M+H]^+$
Elements:		C (0-80); H (0-120); O (0-30); N(0-10); Na (0-5); F(0-5)			
Ion Formula		**Calculated m/z**		**PPM Error**	
C13H11FNO		216.0819		-0.59	

Agilent Technologies

^{1}H NMR of compound **8** in DMSO-*d*6

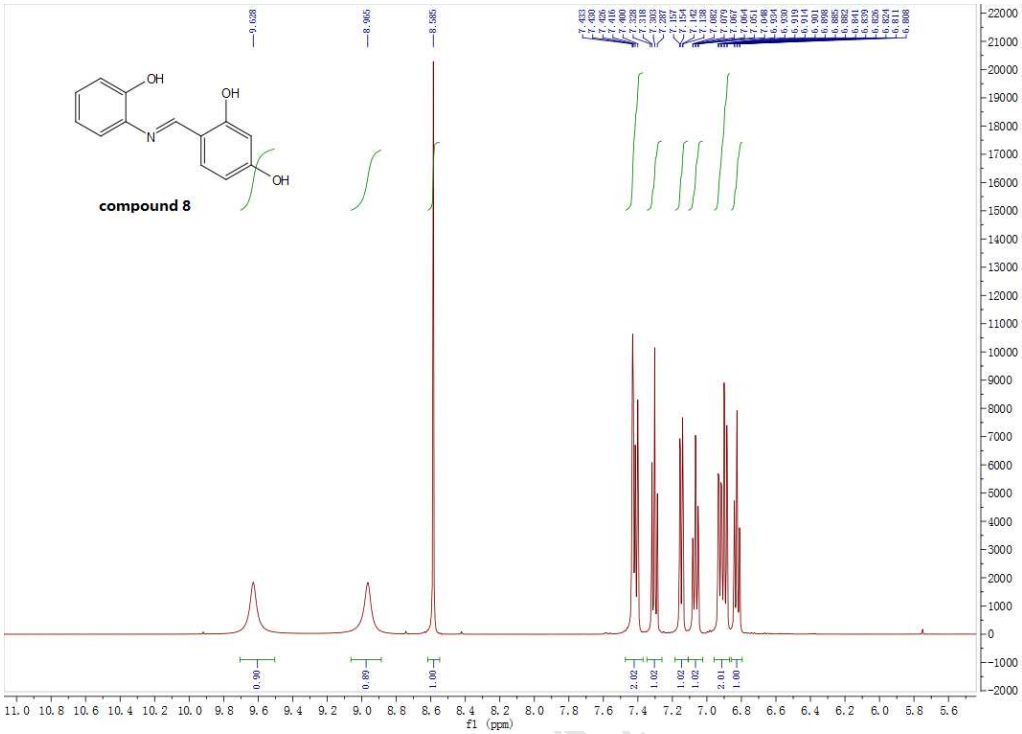

^{13}C NMR of compound **8** in DMSO-*d*6

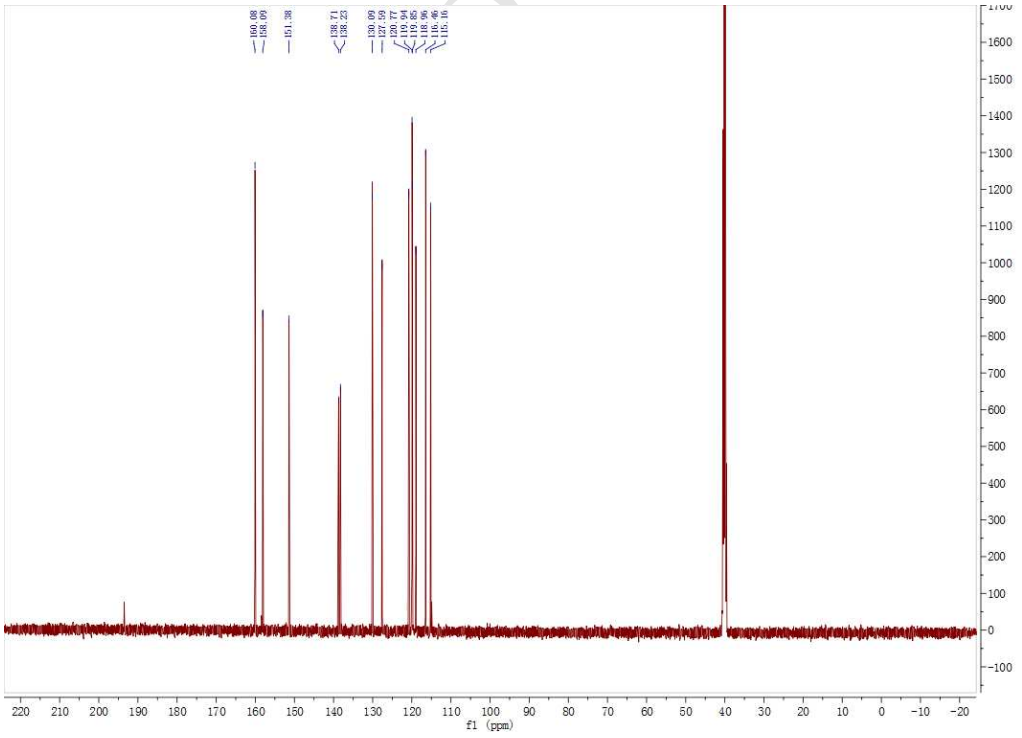

IR of compound **8**

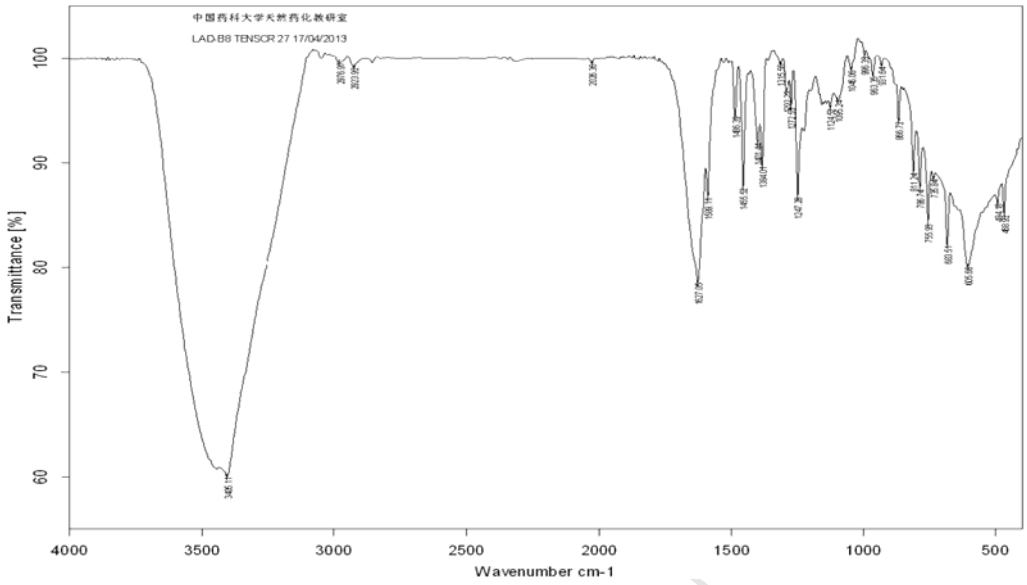

HRMS of compound **8**

TCM-CPU HR-ESI-MS Display Report

Sample Name: Lad-B8 **Instrument:** Agilent 6520B Q-TOF

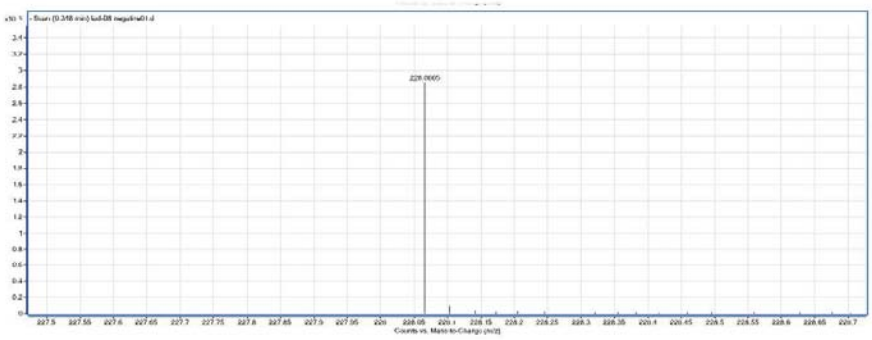

Elemental Composition Calculator

Target m/z:	228.0665	**Result type:**	Negative ions	**Species:**	$[M-H]^-$
Elements:		C (0-80); H (0-120); O (0-30); N(0-10); S(0-5); Cl (0-5)			
Ion Formula		**Calculated m/z**		**PPM Error**	
C13H10NO3		228.0666		0.51	

Agilent Technologies

^{1}H NMR of compound **9** in DMSO-*d*6

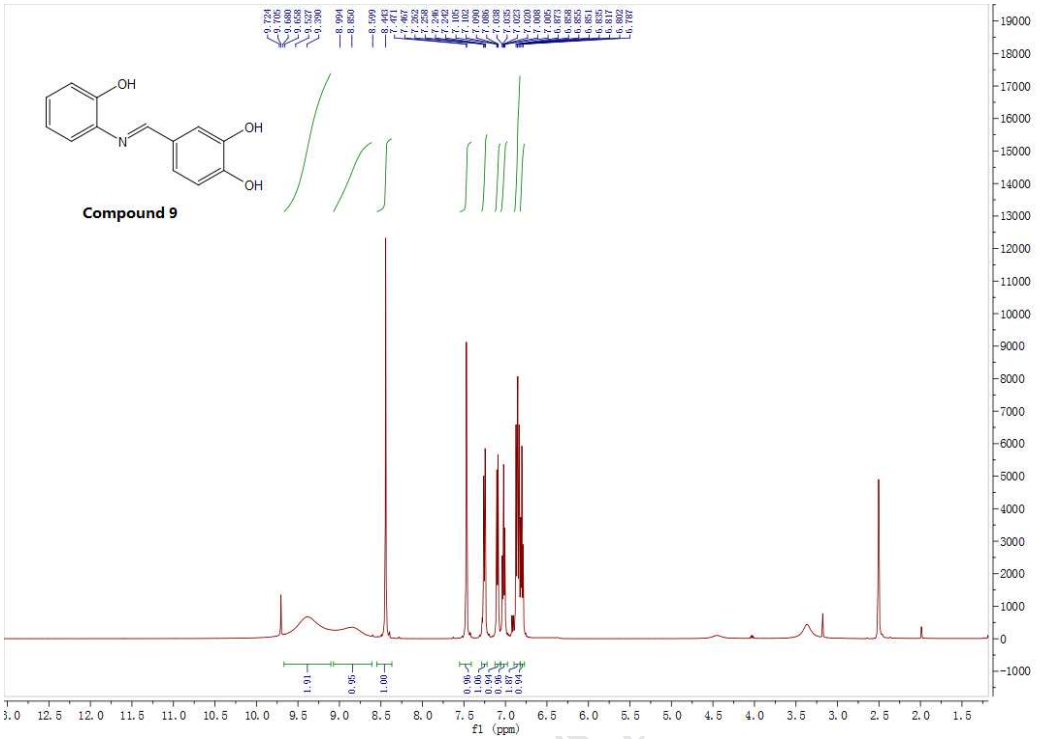

^{13}C NMR of compound **9** in DMSO-*d*6

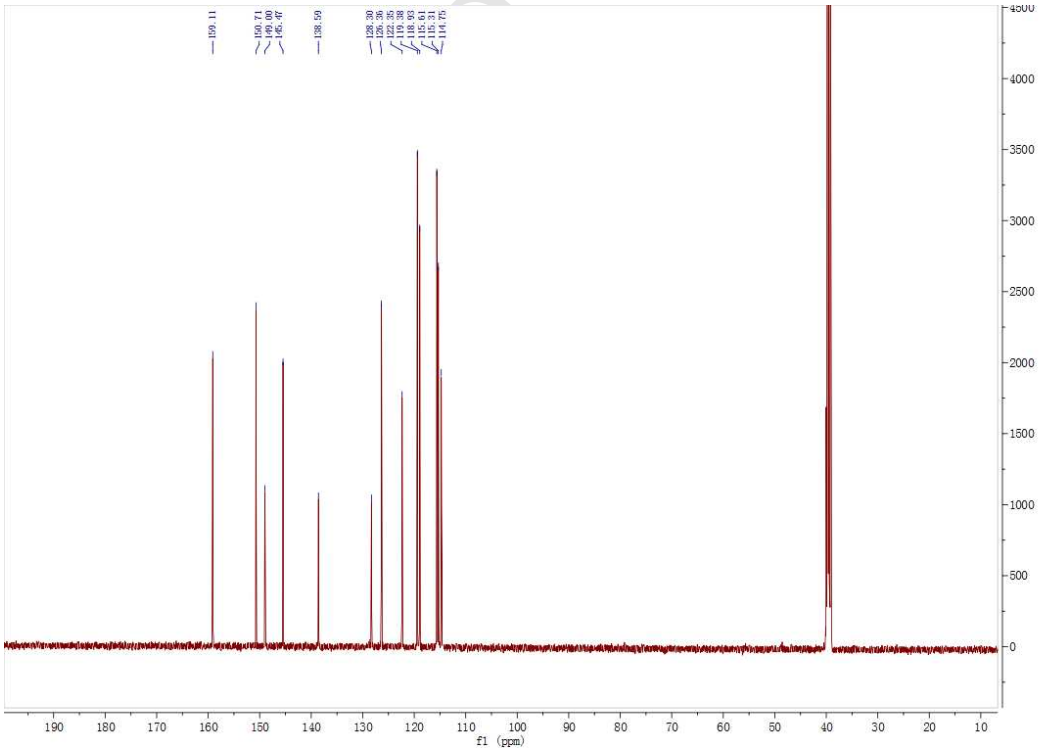

IR of compound **9**

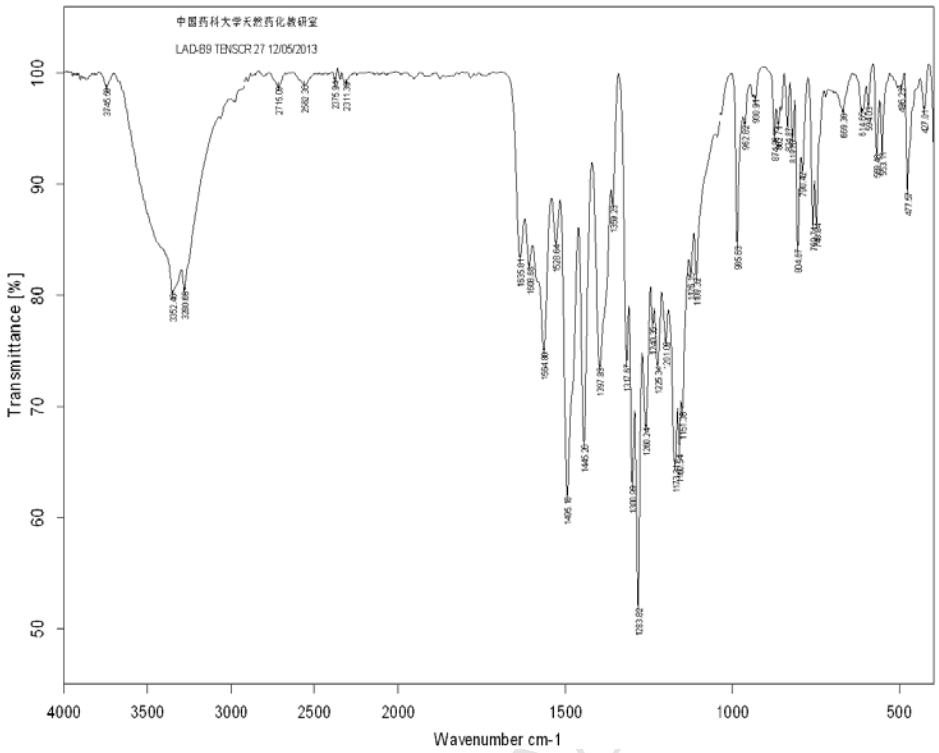

HRMS of compound **9**

TCM-CPU HR-ESI-MS Display Report

Sample Name: Lad-B9 **Instrument:** Agilent 6520B Q-TOF

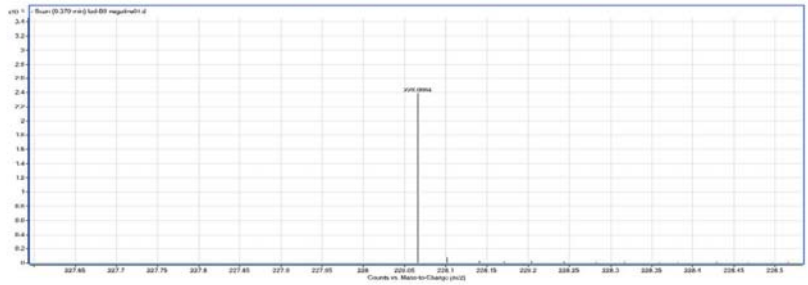

Elemental Composition Calculator

Target m/z:	228.0664	**Result type:**	Negative ions	**Species:**	[M-H]⁻
Elements:		C (0-80); H (0-120); O (0-30); N(0-10); S(0-5); Cl (0-5)			
Ion Formula		**Calculated m/z**		**PPM Error**	
C13H10NO3		228.0666		0.87	

Agilent Technologies

^{1}H NMR of compound **12** in DMSO-*d*6

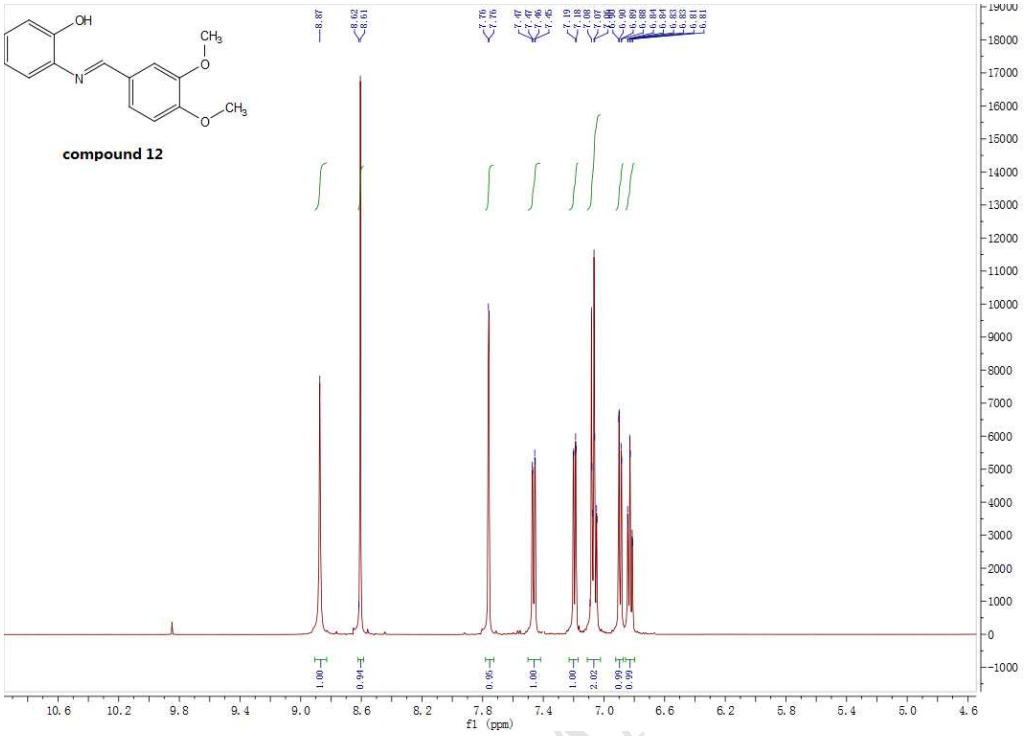

^{13}C NMR of compound **12** in DMSO-*d*6

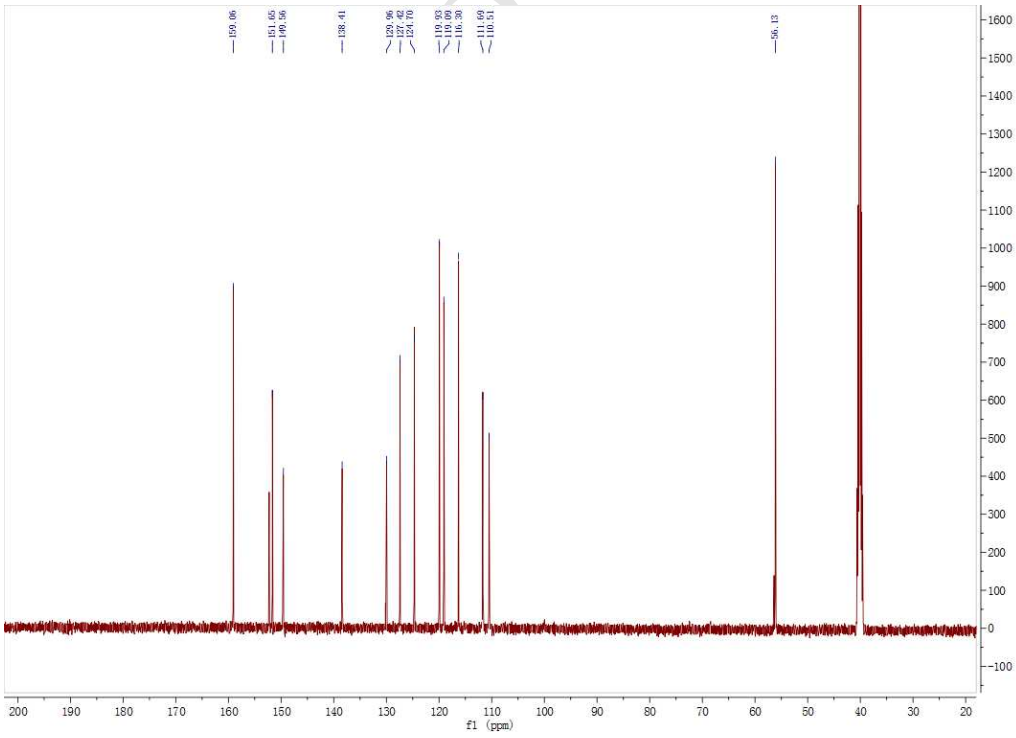

IR of compound **12**

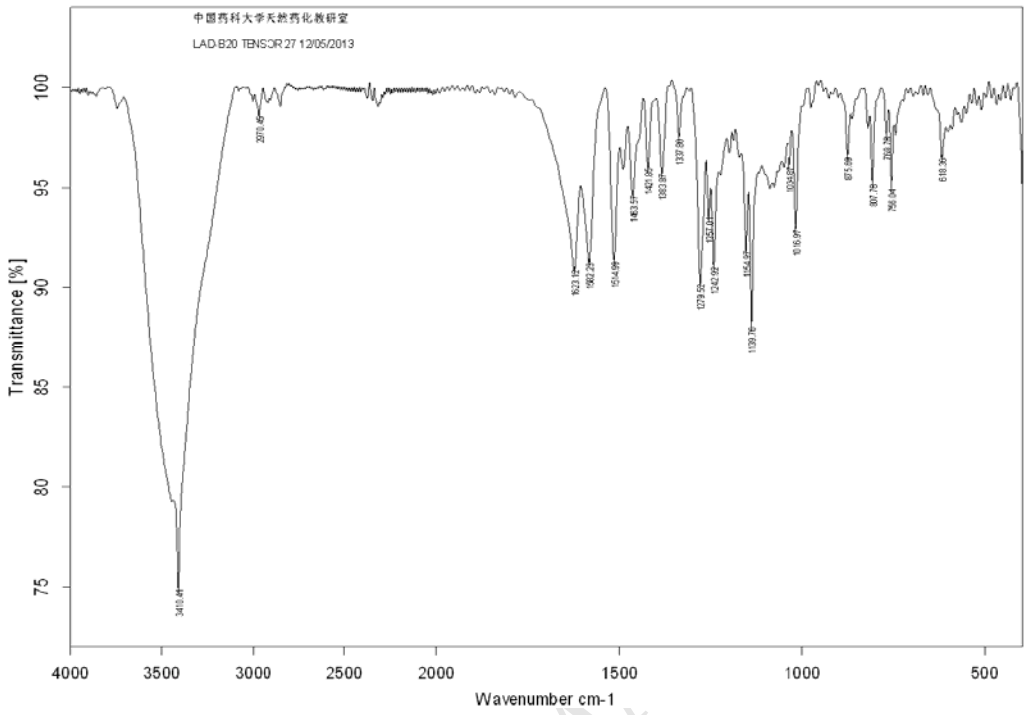

HRMS of compound **12**

TCM-CPU HR-ESI-MS Display Report

Sample Name: Lad-B20 **Instrument:** Agilent 6520B Q-TOF

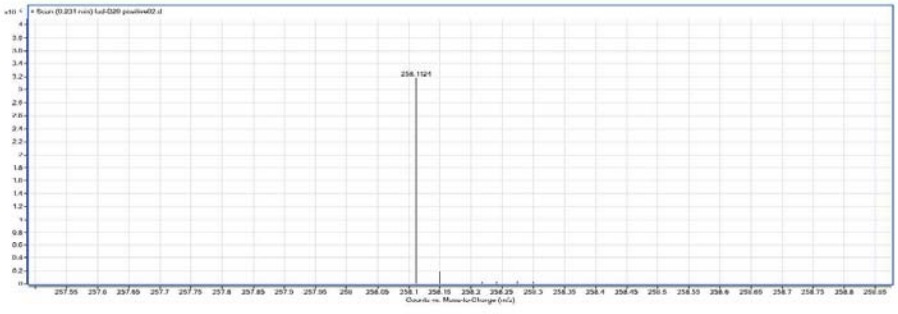

Elemental Composition Calculator

Target m/z:	258.1124	**Result type:**	Positive ions	**Species:**	$[M+H]^+$
Elements:		C (0-80); H (0-120); O (0-30); N(0-10); Na (0-5); F(0-5)			
Ion Formula		**Calculated m/z**		**PPM Error**	
C15H16NO3		258.1125		0.26	

Agilent Technologies

^{1}H NMR of compound **13** in DMSO-*d*6

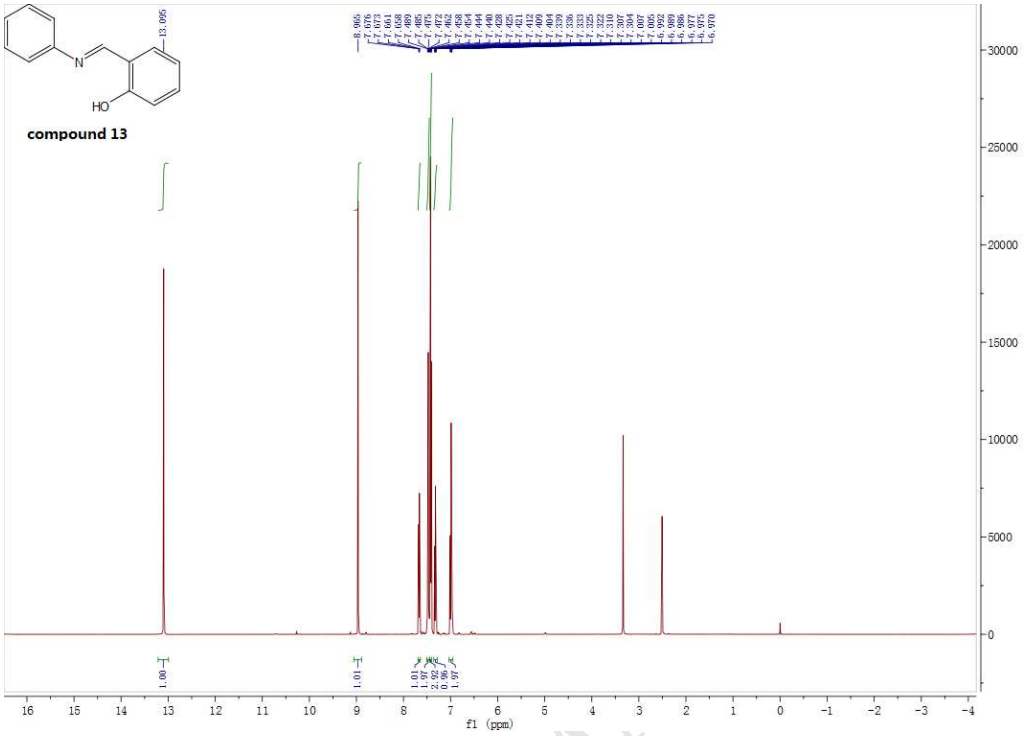

^{13}C NMR of compound **13** in DMSO-*d*6

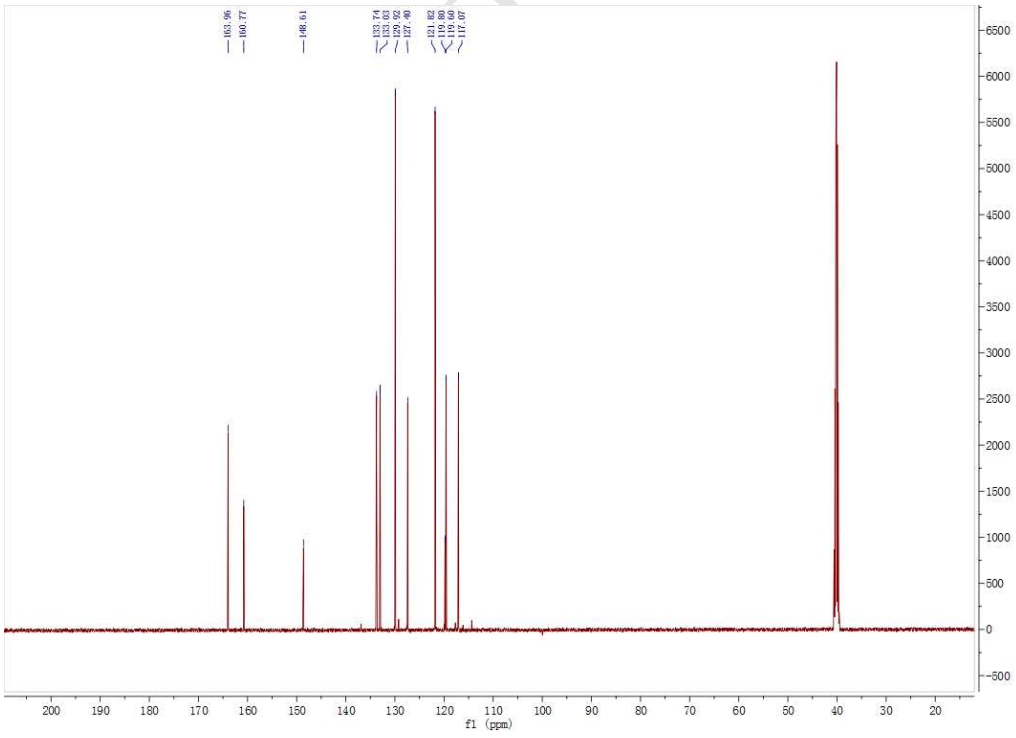

IR of compound **13**

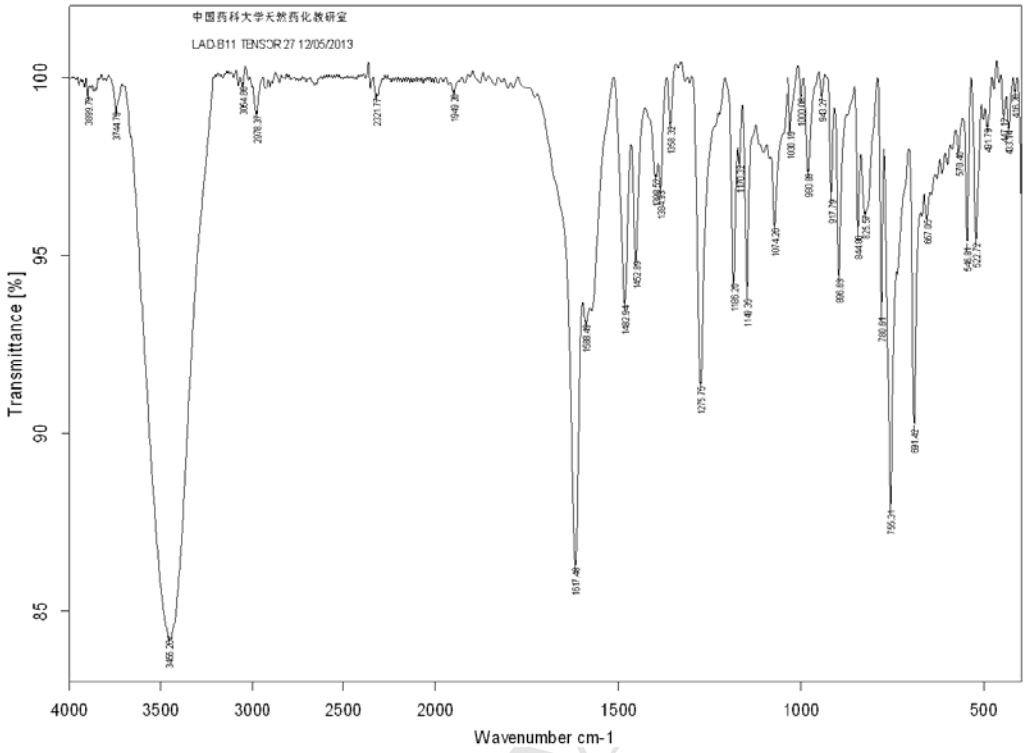

HRMS of compound **13**

TCM-CPU HR-ESI-MS Display Report

Sample Name: Lad-B11 **Instrument:** Agilent 6520B Q-TOF

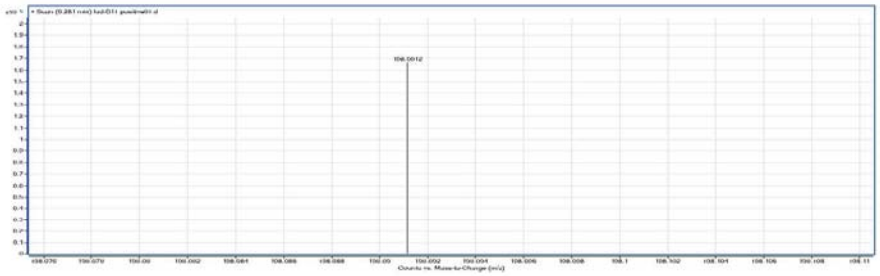

Elemental Composition Calculator

Target m/z:	198.0912	**Result type:**	Positive ions	**Species:**	$[M+H]^+$
Elements:		C (0-80); H (0-120); O (0-30); N(0-10); Na (0-5); F(0-5)			
Ion Formula		**Calculated m/z**		**PPM Error**	
C13H12NO		198.0913		0.84	

Agilent Technologies

^{1}H NMR of compound **14** in DMSO-*d*6

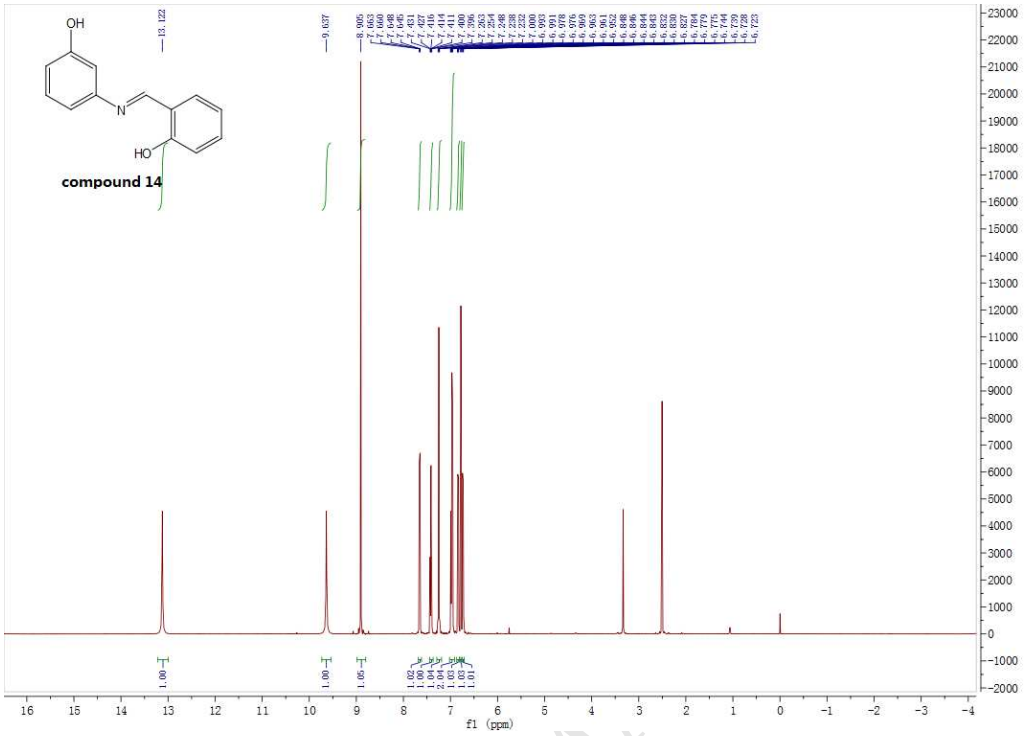

^{13}C NMR of compound **14** in DMSO-*d*6

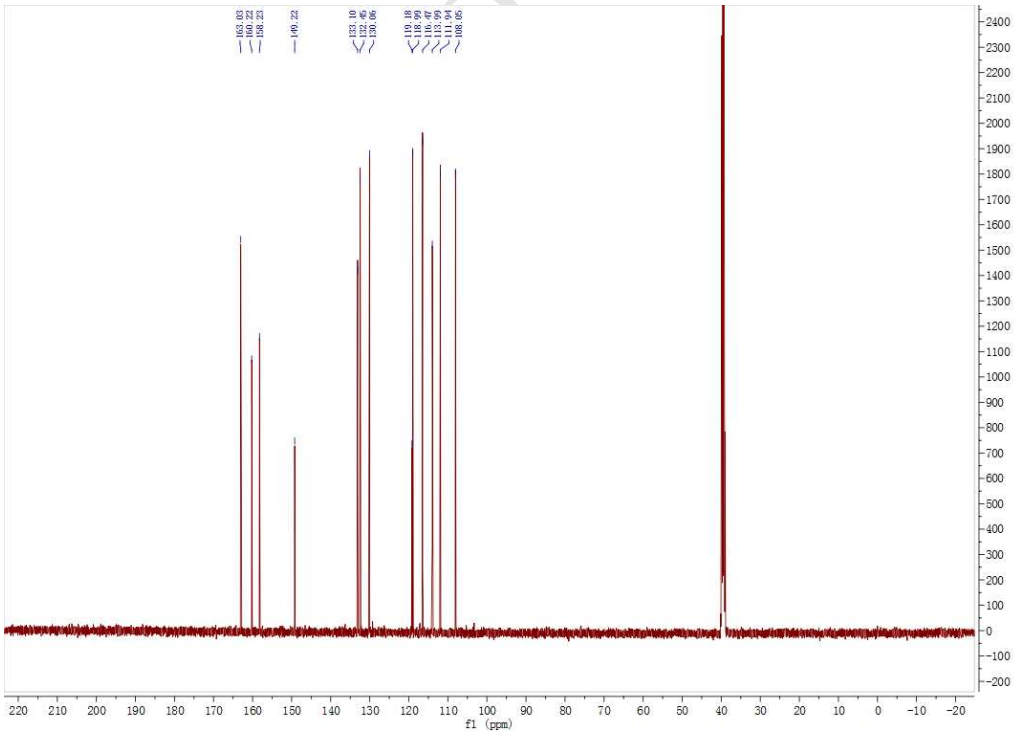

IR of compound **14**

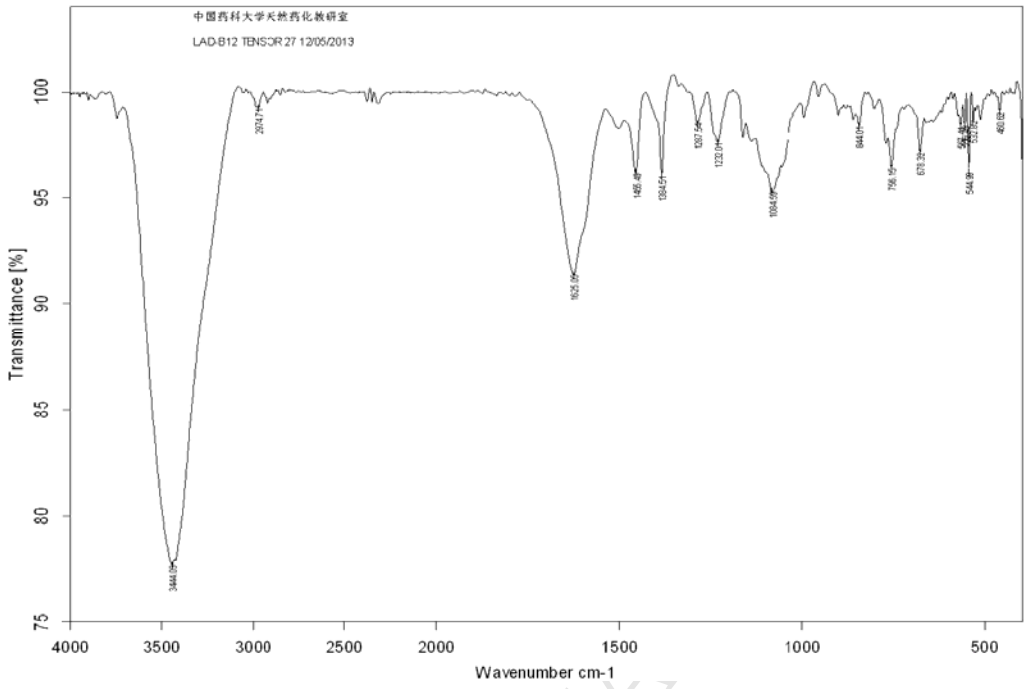

HRMS of compound **14**

TCM-CPU HR-ESI-MS Display Report

Sample Name: Lad-B12 **Instrument:** Agilent 6520B Q-TOF

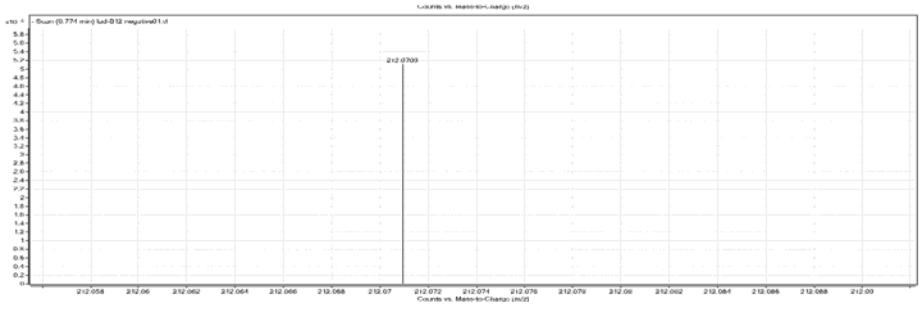

Elemental Composition Calculator

Target m/z:	212.0709	**Result type:**	Negative ions	**Species:**	[M-H]⁻
Elements:		C (0-80); H (0-120); O (0-30); N(0-10); S(0-5); Cl (0-5)			
Ion Formula		**Calculated m/z**		**PPM Error**	
C13H10NO2		212.0717		3.55	

Agilent Technologies

^{1}H NMR of compound **16** in DMSO-*d*6

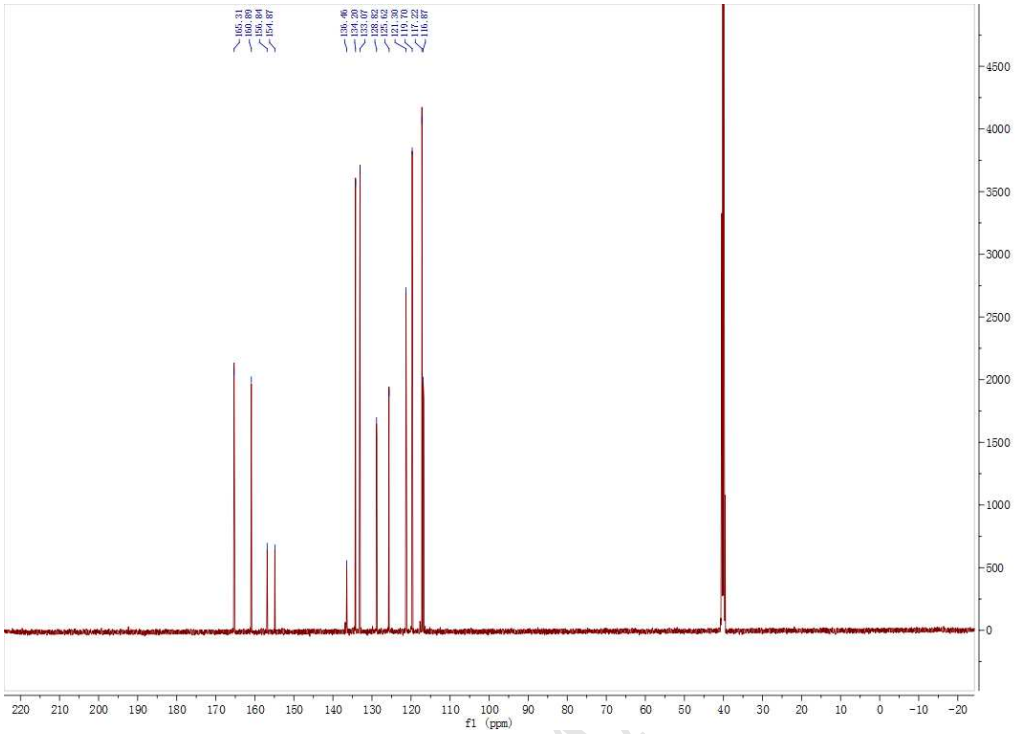

^{13}C NMR of compound **16** in DMSO-*d*6

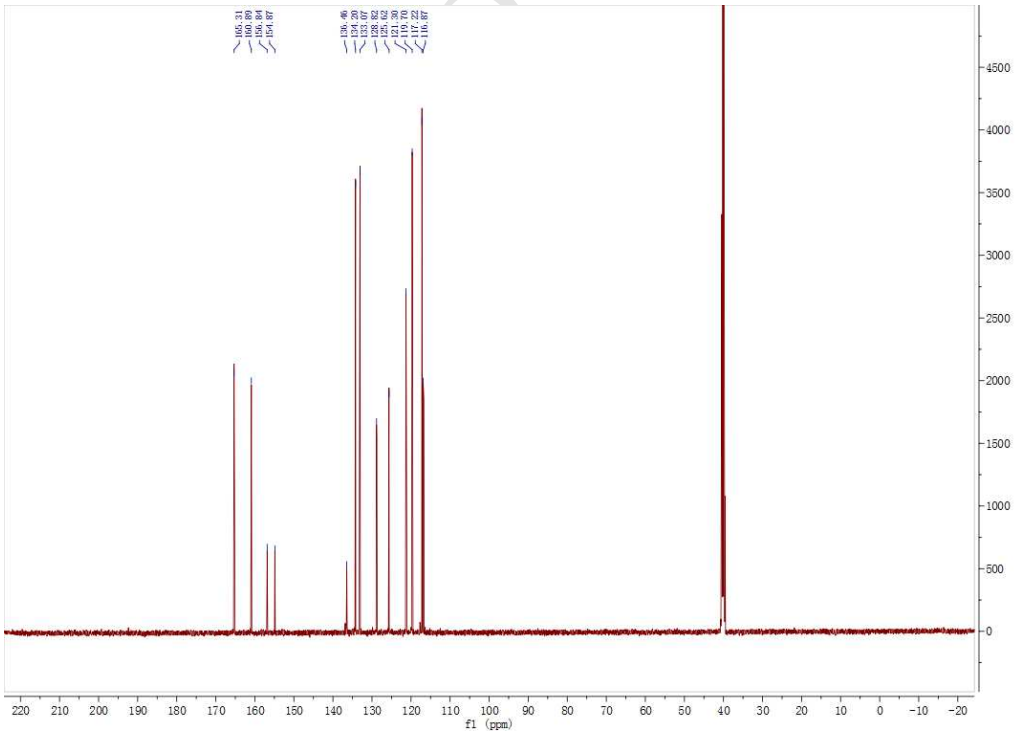

IR of compound **16**

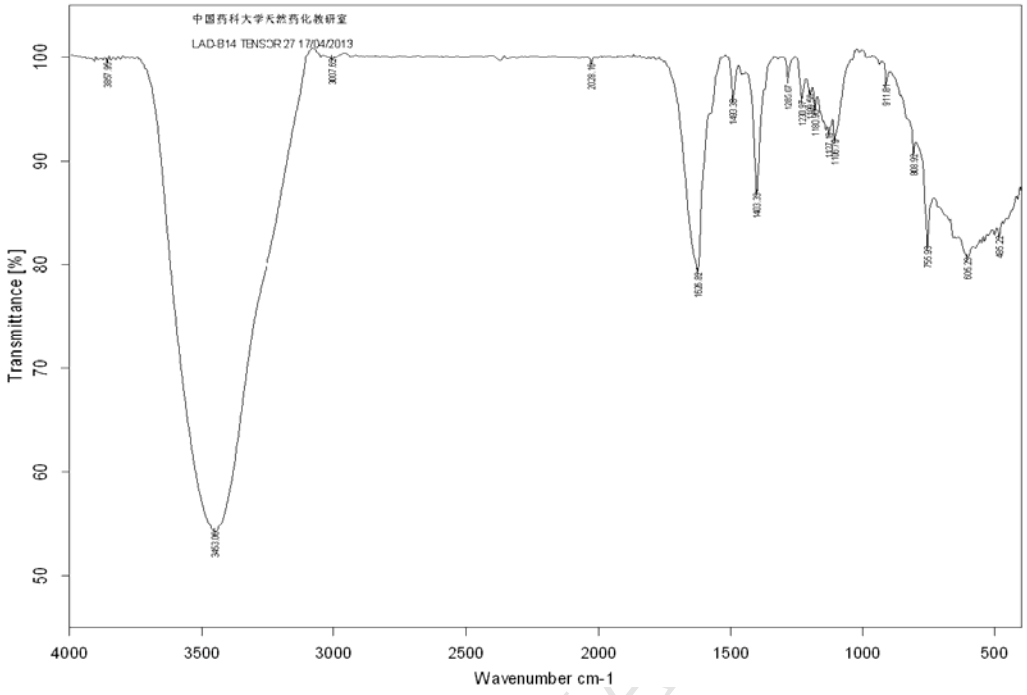

HRMS of compound **16**

TCM-CPU HR-ESI-MS Display Report

Sample Name: Lad-B14 **Instrument:** Agilent 6520B Q-TOF

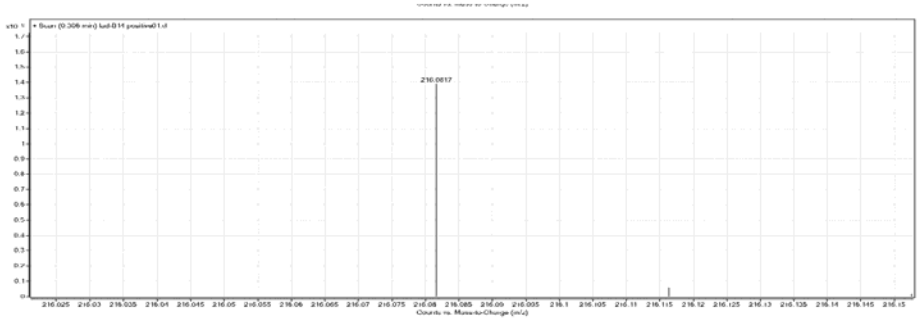

Elemental Composition Calculator

Target m/z:	216.0817	**Result type:**	Positive ions	**Species:**	$[M+H]^+$
Elements:		C (0-80); H (0-120); O (0-30); N(0-10); Na (0-5); F(0-5)			
Ion Formula		**Calculated m/z**		**PPM Error**	
C13H11FNO		216.0819		1.04	

Agilent Technologies

^{1}H NMR of compound **19** in DMSO-*d*6

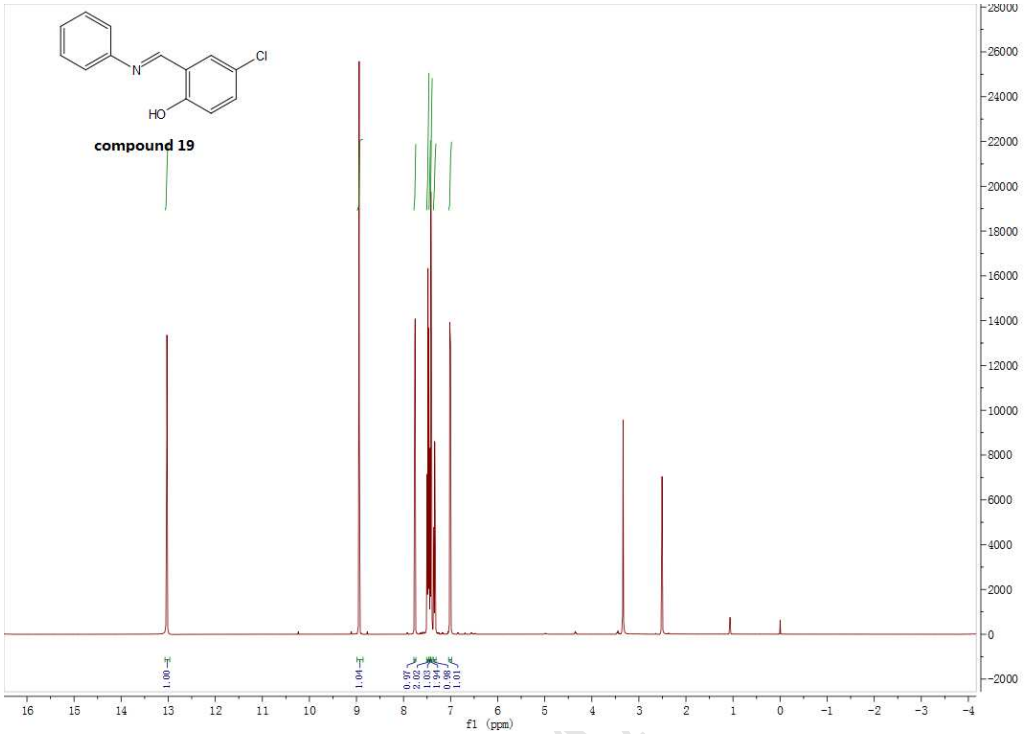

^{13}C NMR of compound **19** in DMSO-*d*6

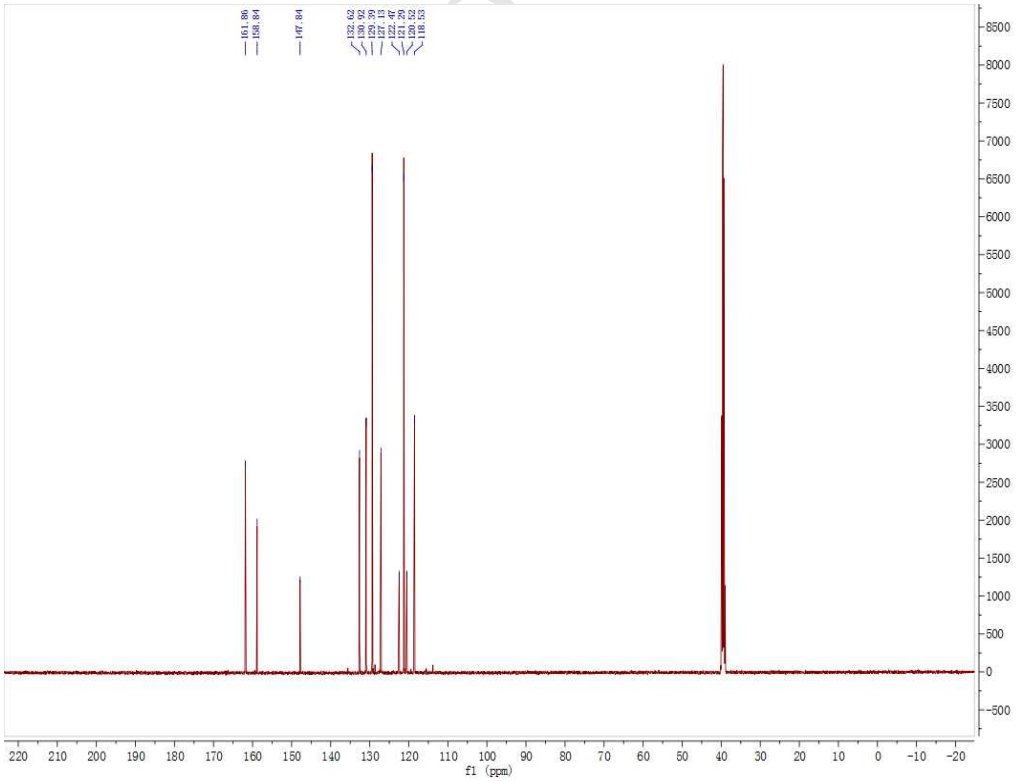

IR of compound **19**

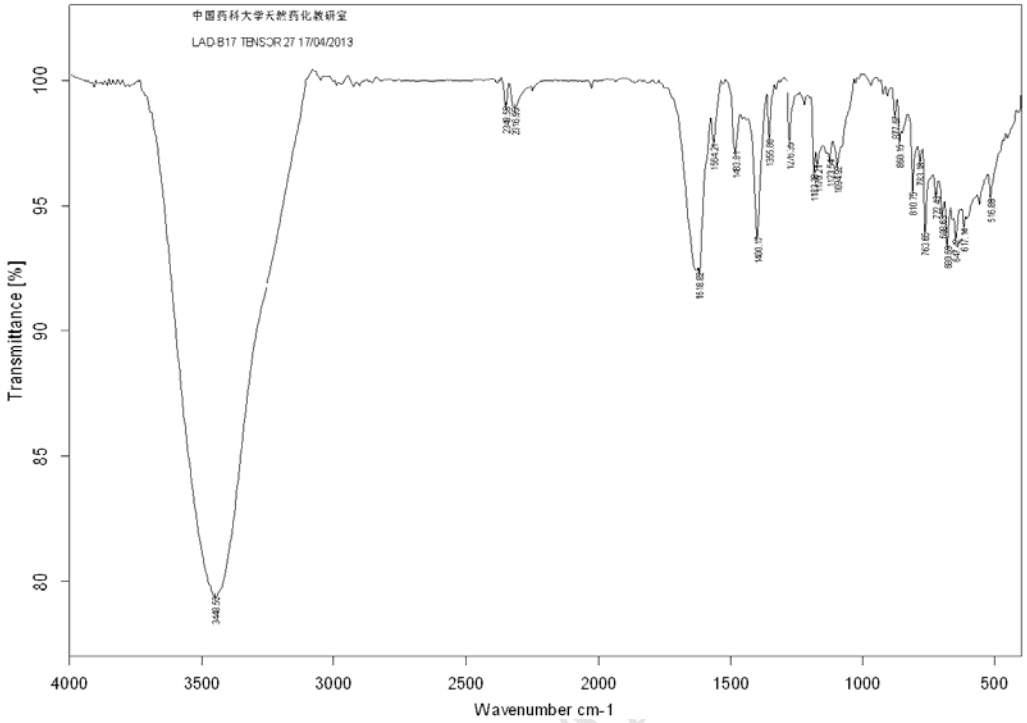

HRMS of compound **19**

TCM-CPU HR-ESI-MS Display Report

Sample Name: Lad-B17 **Instrument:** Agilent 6520B Q-TOF

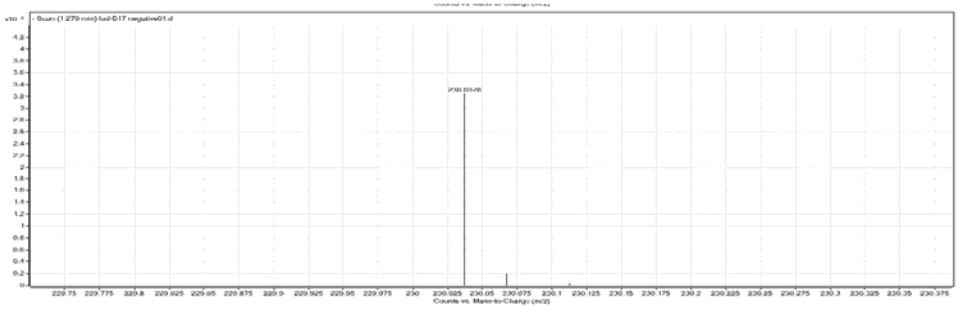

Elemental Composition Calculator

Target m/z:	230.0376	**Result type:**	Negative ions	**Species:**	[M-H]⁻
Elements:		C (0-80); H (0-120); O (0-30); N(0-10); S(0-5); Cl (0-5)			
Ion Formula		**Calculated m/z**		**PPM Error**	
C13H9ClNO		230.0378		1.15	

Agilent Technologies

^{1}H NMR of compound **20** in DMSO-*d*6

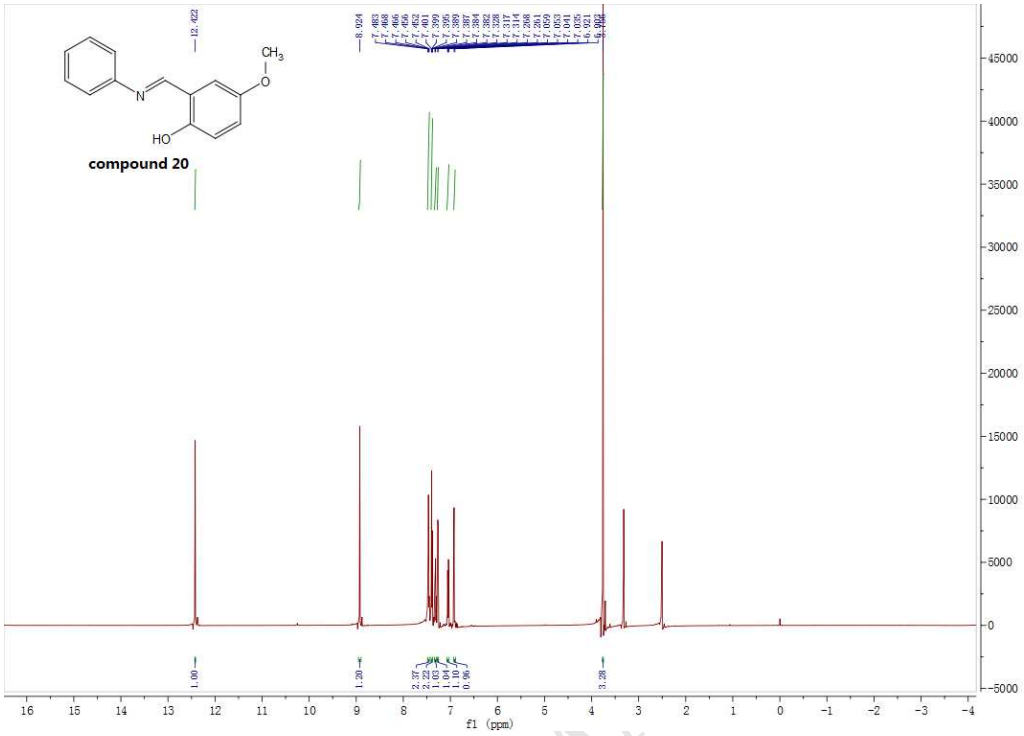

^{13}C NMR of compound **20** in DMSO-*d*6

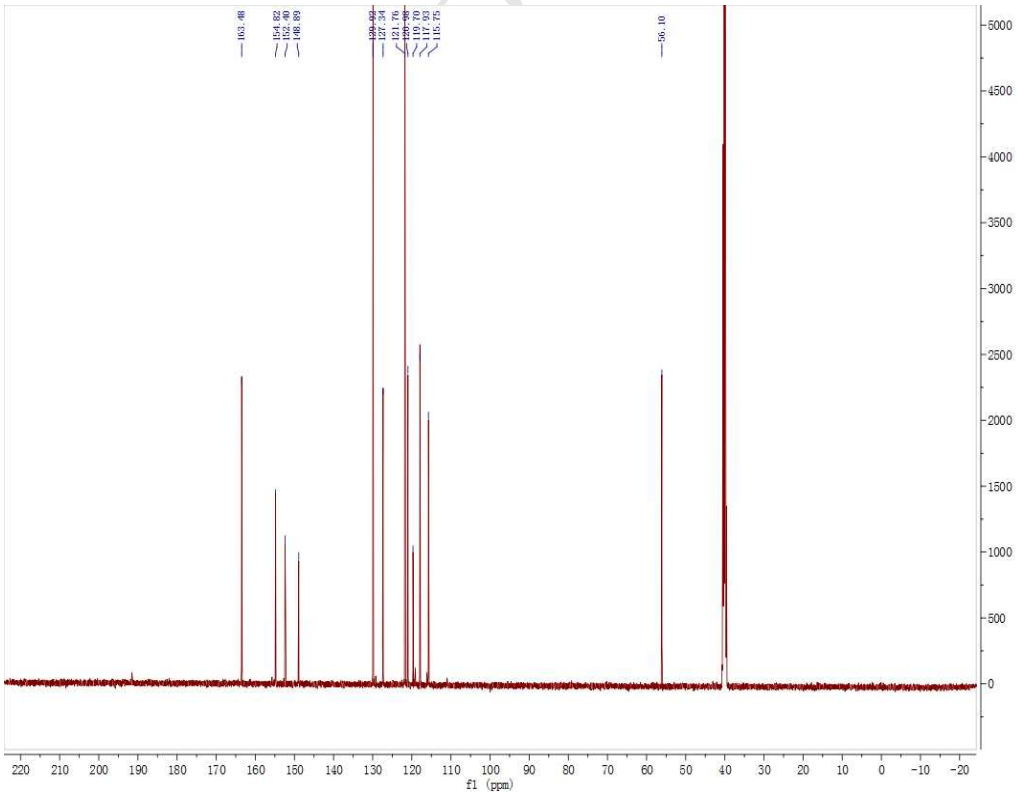

IR of compound **20**

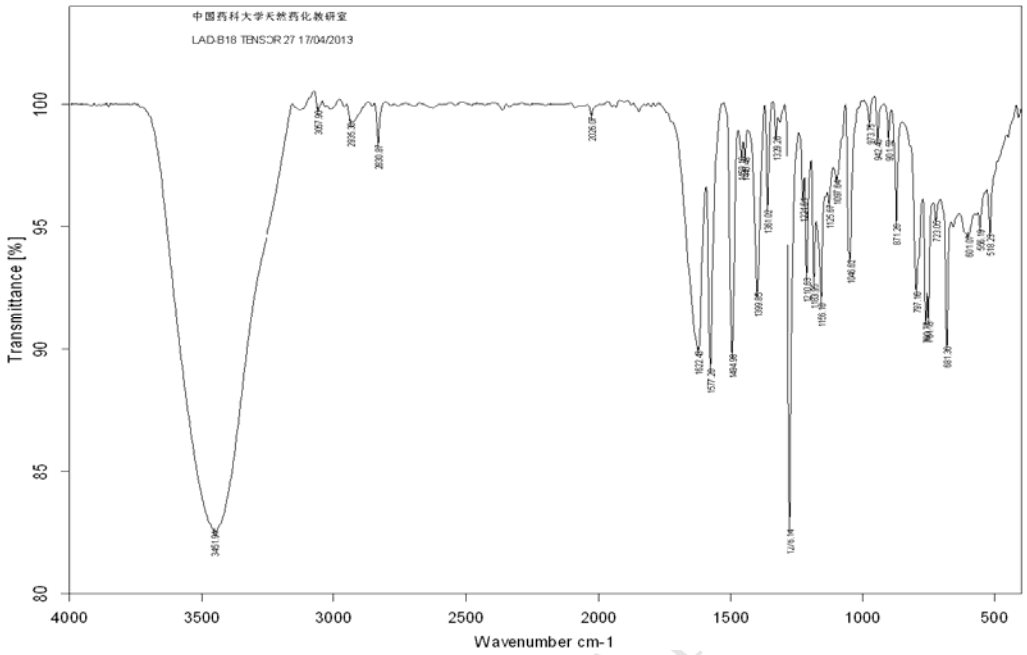

HRMS of compound **20**

TCM-CPU HR-ESI-MS Display Report

Sample Name: Lad-B18 **Instrument:** Agilent 6520B Q-TOF

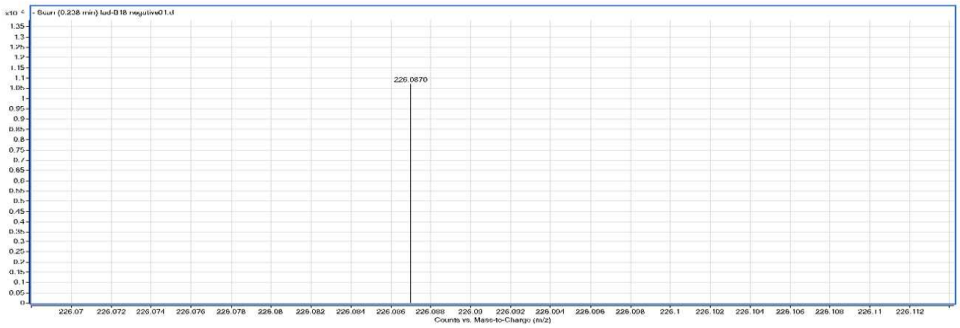

Elemental Composition Calculator

Target m/z:	226.0670	**Result type:**	Negative ions	**Species:**	$[M-H]^-$
Elements:		C (0-80); H (0-120); O (0-30); N(0-10); S(0-5); Cl (0-5)			
Ion Formula		**Calculated m/z**		**PPM Error**	
C14H12NO2		226.0674		1.51	

Agilent Technologies